ABSTRACT

Title of Document:	SPILL AND BURNING BEHAVIOR OF FLAMMABLE LIQUIDS
	Matthew E. Benfer, Master of Science in Fire Protection Engineering, 2010
Directed By:	John L. Bryan Professor, James G. Quintiere, Department of Fire Protection Engineering

Unconfined liquid spill depths were measured for two liquid fuels and three non-flammable liquids atop a smooth concrete pad. Unconfined liquid spill thicknesses were found to be less than 0.1 cm in all fuels and liquids similar to fuels. Spill fires were conducted with volumes ranging from 0.2 ml to 450 ml for gasoline and denatured alcohol. Average burning rates for both unconfined liquid fuel spill fires increased linearly with increasing volume spilled. A liquid spill thickness model was developed and compared to experimental data. Comparisons showed good predictions for half of the liquids used. In addition, a liquid spill fire burning rate model was also developed and checked with experimental data. This model provided good qualitative results, however further development is still needed.

SPILL AND BURNING BEHAVIOR OF FLAMMABLE LIQUIDS

By

Matthew E. Benfer

Thesis submitted to the Faculty of the Graduate School of the
University of Maryland, College Park, in partial fulfillment
of the requirements for the degree of
Master of Science
2010

Advisory Committee:
Professor James G. Quintiere, Chair
Daniel T. Gottuk
Marino di Marzo

Acknowledgements

This project was supported in part by Award No. 2008-DN-BX-K168 awarded by the National Institute of Justice, Office of Justice Programs, U.S. Department of Justice (DOJ) under management of Dr. Daniel Gottuk. In addition the assistance given from Dr. James Quintiere and the Fire Protection Engineering department of the University of Maryland allowed me to complete the testing for this thesis.

I would like to express my gratitude to the employees of the ATF Fire Research Lab in Beltsville, MD and student Tom Layton for their assistance in setup and running of all of my experiments.

I would also like to thank my advisor at Hughes Associates, Dr. Gottuk, and my co-worker, Chris Mealy, for their aid and support of my work. Their insight has helped guide me through this project.

My faculty advisor, Dr. James Quintiere has helped me build the foundation of this project. With his direction, I was able to learn and accomplish more than I thought possible.

Lastly, I would like to thank my family for their support throughout my academic career. Without them, I would not have reached this far.

Table of Contents

List of Tables

List of Figures

Nomenclature

A	-	Area	(m^2)
α	-	Thermal Diffusivity	(m^2/s)
B	-	Spalding B Number	-
β	-	Expansion Coefficient	(1/K)
c_p	-	Specific Heat	(kJ/kg-K)
δ	-	Spill Thickness	(cm)
δ_{inf}	-	Asymptotic Spill Depth	(cm)
$\mathfrak{D}$	-	Dimensionless Diameter	-
D	-	Diameter	(m)
$\Delta\tau$	-	Dimensionless Time Step	-
ε	-	Exponential Spill Depth Factor	(ml^{-1})
g	-	Gravitational acceleration	(m/s^2)
γ	-	Dimensionless Constant	-
h_c	-	Convective Heat Transfer Coefficient	(W/m-K)
h_{fg}	-	Heat of Vaporization	(lJ/kg)
k	-	Thermal Conductivity	(W/m-K)
$\kappa\beta$	-	Extinction Coefficient/Mean Beam Length Correction	(m^{-1})
L	-	Latent Heat of Gasification	(kJ/kg)
λ	-	Characteristic Time Ratio	-
m	-	Mass	(kg)
$\dot{m}_f$	-	Fuel Burning Rate	
$\dot{m}_f''$	-	Fuel Burning Rate Per Unit Area	($kg/s\text{-}m^2$)
$\dot{m}_{max}''$	-	Maximum Burning Rate Per Unit Area	($kg/s\text{-}m^2$)
ν	-	Kinematic Viscosity	(m^2/s)
Nu	-	Nusselt Number	-
θ	-	Contact angle	(^{o})
$\dot{q}_{net}''$	-	Conduction Heat Flux	(W/m^2)
$\dot{q}_k''$	-	Net Flame Heat Flux	(W/m^2)
q_o	-	Convective Burning Rate Constant	($kg/s\text{-}m^{7/4}$)
ρ	-	Density	(kg/m^3)
R	-	Thermal Resistance	(m^2-K/W)
Ra	-	Rayleigh Number	-
σ	-	Surface Tension	(N/m)

σ_{sl}	-	Solid-Liquid Interfacial Tension	(N/m)
σ_{sv}	-	Solid-Vapor Interfacial Tension	(N/m)
τ	-	Dimensionless Time	-
T	-	Time	(s)
T_{∞}	-	Ambient temperature	(K)
T_b	-	Boiling Temperature	(K)
t_e	-	Characteristic Evaporation Time	(s)
t_k	-	Characteristic Conduction Time	(s)
T_s	-	Surface Temperature	(K)
V	-	Liquid Volume	(ml)
ψ	-	Dimensionless Constant	-

Subscripts

i	-	Initial
l	-	Liquid
s	-	Solid

1 Introduction

1.1 Motivation

In many applications and circumstances, a liquid spill fire or liquid pool fire is a likely hazard. From industrial liquid spills to commercial or residential arson cases, flammable liquid spills and pools pose a great danger to property and human safety. However, only the burning behavior of confined liquid pan fires is well characterized. There is not presently a model or correlation for accurately predicting the burning behavior of an unconfined instantaneous flammable liquid spill fire. Some current methods, [Iqbal et al, 2004], use pool fire correlations to determine the heat release rate for a spill fire with a prescribed area. This tends to over-estimate the heat release rate and under-estimate the burning duration for a given fuel volume. It is often difficult to model a liquid fuel fire without considering one at steady-state because of the wide range of scenarios and the large amount inherent complexities involved with these types of fires, especially spill fires. Figure 1-1 shows an event tree that can be used for characterizing the development of different types of liquid fuel fires. Notice that there are multiple tiers, each representing a certain aspect of the fire. Each tier has multiple alternatives in it, creating a vast number of scenario combinations, some of which are omitted for simplicity. Every scenario in this tree would potentially have a different physical model. The path noted in bold is the fuel spill fire scenario that will be covered in this research.

It is important to differentiate between a liquid pool fire and a liquid spill fire, because both represent vastly different scenarios. A liquid pool is considered to be a layer of liquid generally greater than 1 cm [SFPE, 2002] that is bounded by walls or

some other physical boundary, while an unconfined liquid spill is not bounded by physical boundaries. This unbounded nature of a liquid spill would result in a much thinner layer of liquid, on the order of 0.1 cm [SFPE, 2002]. The knowledge of how to address and evaluate the differences between liquid pool fires and liquid spill fires will be very beneficial in understanding the hazards posed by these types of fire scenarios.

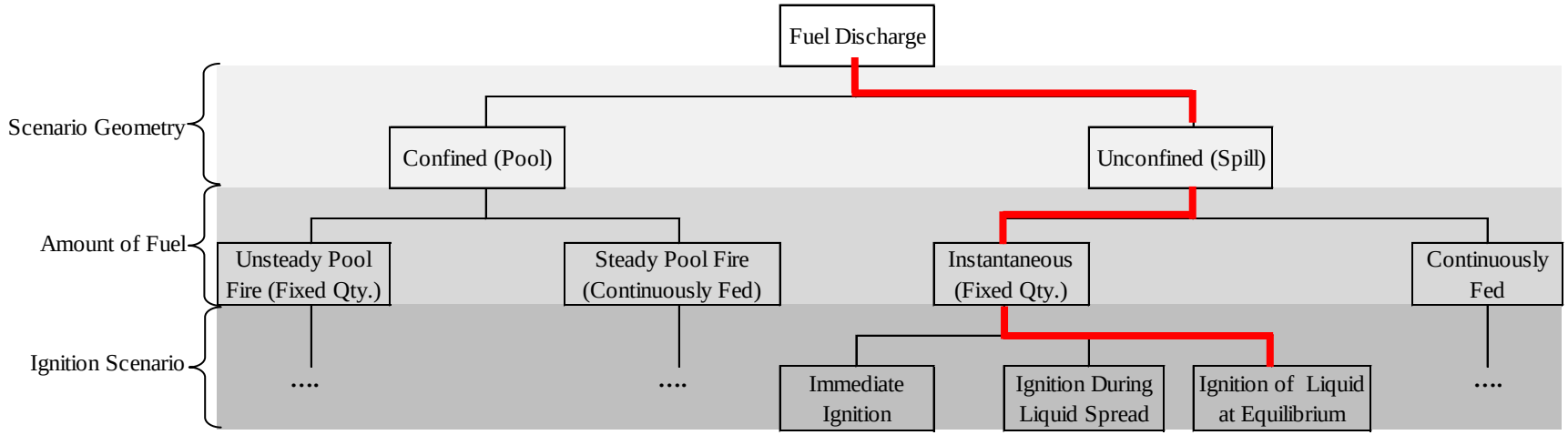

Figure 1-1 - Event tree following a fuel discharge

1.2 Objectives

At present, there lacks a conclusive model for determining the burning dynamics of an instantaneous flammable liquid spill. This is because liquid fuel spill fires are highly transient phenomena with many unknowns that could affect the fire behavior. In order to construct a model to describe a flammable liquid spill fire, one must couple a model that describes liquid spread with a spill burning rate model. The objective of this work is to create a framework for assessing the hazard of a fuel spill fire through the use and development of one such model. This methodology is structured in the following manner:

1. Assess the unconfined spreading dynamics of fixed quantities of various liquids, both flammable and non-flammable, over a flat surface.
2. Determine the burning behavior of flammable liquids spilled on an unconfined flat surface.
3. Develop and validate a model to describe liquid spill thickness.
4. Develop and validate a model to describe the burning rate of a liquid spill fire.

2 Background on Liquid Spills and Burning Rate

2.1 Liquid Spread

The focus of this research is to address fixed quantity, unconfined liquid spills. A liquid spill is considered to be unconfined when the liquid spread is not impeded by a physical boundary such as a wall. Another constraint on the spill type being discussed in this work is that the method of spill should be quasi-instantaneous.

That is to say that there is a fixed quantity of liquid which is spilled in a short period of time. While other types of spills such as continuously fed spills are not the main focus of this research, they will be discussed as they relate to instantaneous spills.

As a liquid is spilled and spreads, it will undergo three physical regimes governing the motion and equilibrium state of the fluid. These regimes, as outlined in the research of Putorti et al. [2001], are gravity-inertia, gravity-viscous, and viscous-surface tension. The regimes are named by the force that tends to spread the liquid and the force that tends to oppose spread, respectively. Due to the forces within a spreading liquid, unconfined spills tend to ideally have the shape of a flat disc with a uniform thickness. This spill thickness becomes an important parameter when discussing the hazard of an unconfined liquid spill. Simmons et al. [2004] found typical spill thicknesses for various types of liquids including antifreeze, mineral oil, and motor oil to be between 0.048 cm and 0.16 cm. Water was an outlier in this study, having a spill depth of approximately 0.34 cm.

Much work has been done in the fields of lubrication, film coatings, and surface wetting on the spread of liquids over a surface, either solid or liquid. Analytical solutions to the problem of liquid spread tend to take one of two approaches: either a dynamic approach or an equilibrium approach for determining liquid spread. The liquid spread can be characterized either by a liquid thickness or length scale such as diameter of spread. As a note, most analytical solutions assume a liquid is spilled on an impermeable and completely flat surface. Including the effects of permeability and non-level surfaces would greatly complicate the governing

equations and result in equations that cannot be solved analytically. Studies that have conducted research on spills on permeable substrates will be discussed later.

Analytical equations describing the time dependent fluid spread over a flat impermeable surface have been found by Raj et al. [1974] and Grimaz et al. [2007], among others. The general method for determining these solutions is to represent each of the three liquid spread regimes; gravity-inertia, gravity-viscous, and viscous-surface tension with a set of physical equations representing the regime. Then, the equations would be solved analytically. This results in a spill length scale, typically diameter or radius of spread, as a function of time for each regime as well as the times to reach each regime. Equations produced by this type of derivation tend to be somewhat similar and require properties of the fluid (density, viscosity, etc.) as well as the spill configuration (flow rate, source geometry, etc.). This allows for the modeling of various types of spills, whether instantaneous or continuous.

Calculating spill thickness at equilibrium is a much more simple case to solve. Such a method was used by Bradley [2002] and Simmons et al. [2004] with minor differences in the two equations. The basis for these derivations is a thermodynamic approach which solves a balance of surface tension and pressure forces along a fluid's curved surfaces, found in Batchelor [1967]. Another method by Vignes-Adler [2002] produces the same result as Bradley [2002] in a much more compact manner using a force balance in a large liquid drop. The resulting equation will be presented later.

These two types of analytical methods for characterizing liquid spills require vastly different parameters. The dynamic fluid spread models require liquid and spill configuration properties, while the equilibrium spill thickness model requires a

smaller set of liquid and liquid-substrate properties. Both methods provide useful information about the behavior of liquid spills and the choice of method depends on the configuration in question and the desired result.

Sources such as Modak [1981], Simmons et al. [2004], and Putorti et al. [2001] state that for an unconfined spill, the resulting equilibrium spill thickness on a flat impermeable surface is independent of the volume of liquid spilled. The two types of methods noted above yield different outcomes: either a spill thickness dependent on time, or an equilibrium spill thickness. If a closer look is taken at the time dependent results of Raj et al. [1974] and Grimaz et al. [2007], one finds that the spills have a tendency towards spreading that becomes very slow at some point, yielding a quasi-equilibrium spill thickness. However, when using these transient solutions, the resulting quasi-equilibrium spill thickness is not necessarily shown to be independent of the volume spilled. A possible reason for this is that the solutions do not take into account adhesion phenomena at the liquid-solid interface such as contact angle, which provides a means for the spill to come to equilibrium. On the other hand, the results of the equilibrium method explicitly show that there is no impact of volume of the spill on the spill thickness. One useful part of the transient models in Raj et al. [1974] and Grimaz et al. [2007] is that they show how certain liquid properties influence the spread of a liquid. For instance, keeping all other parameters constant, increasing the fluids viscosity will tend to slow the liquid spread.

When discussing a liquid spill, one must first explore the surface wetting phenomena of a small liquid drop. When a liquid drop is placed on a flat solid surface it tends to spread to equilibrium in a shape dependent on liquid and surface properties

[Vignes-Adler, 2002]. This shape is either a sessile drop (partial wetting) or a thin film (total wetting), seen in Figure 2-1. A liquid will tend to make this shape in order minimize surface energy. The point where the solid, liquid, and gas phases meet is called the triple point. At this point, the liquid surface makes an angle with the solid surface, called the contact angle θ (Figure 2-1). The contact angle controls the shape of the drop on the surface. Total wetting occurs when this contact angle is very close to zero. As the volume of a partial-wetting drop increases, in order to satisfy equilibrium conditions at the edge, the drop grows in area and the center of the drop becomes flat (Figure 2-2).

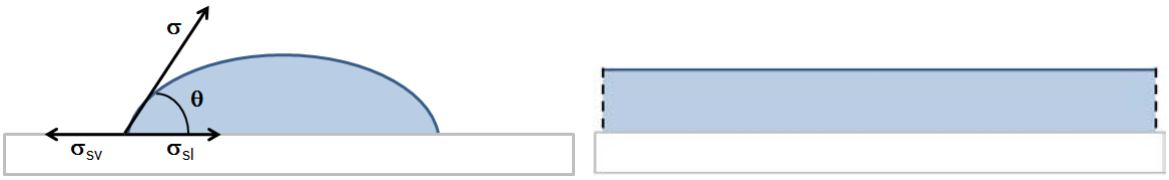

Figure 2-1 - Partial (left) and total (right) wetting of a liquid drop on a solid surface

Figure 2-2 - Partial wetting of a large drop

A liquid spill behaves much the same as a large liquid drop in the case where the liquid partially wets the surface, which is common for most liquids. In particular, the edges of a liquid spill behave the same as drops, allowing methods for determining droplet equilibrium to be used for larger liquid spills.

The contact angle of the liquid-substrate interface has a large impact on the equilibrium drop height equation found in Vignes-Adler [2002] and should be explored. Contact angle is typically determined experimentally, but can be related to the interfacial tensions of the liquid-air (typically referred to as the surface tension of a liquid, σ), solid-liquid (σ_{sl}), and the solid-gas or surface free energy (σ_{sv}), using Young's Law, equation (1):

$$\cos(\theta) = (\sigma_{sv} - \sigma_{sl})/\sigma \tag{1}$$

Interfacial tension is a measure of the adhesive forces that occur between two substances; solid, liquid, or gas. The units of interfacial tensions are typically reported in N/m, which is a measure of force per unit length. The interfacial tension between a liquid and air is typically referred to as the surface tension of a liquid and is the only one of the three values in equation (1) that is typically known for a liquid-substrate system. The surface tension of a liquid is relatively easy to measure experimentally, while the solid-liquid and solid-gas interfacial tensions are much more difficult. Because the contact angle is also relatively easy to find experimentally, knowing this and the surface tension, one could solve for the difference between the interfacial tensions using Young's law. The Young's Law relation is valid for the ideal case of a liquid resting on an impermeable and perfectly flat surface.

2.1.1 Surface Permeability and Liquid Absorption

Most surfaces found in typical industrial and commercial applications are not ideal; neither perfectly flat nor perfectly impermeable. Therefore, it is important to

understand the effects that the various surface characteristics have on liquid spread. Some work has been done to analyze the impact of permeability on liquid spread. Keller et al. [2005], Simmons et al. [2004], and Belore et al. [1988] examined the effects of substrate permeability on liquid spread. These studies were mainly concerned with substrates such as pavements, soils, and snow. However, the results obtained can be applied to most permeable surfaces. The permeability, or tendency for a certain liquid to penetrate into a porous surface, is a property determined by the surface and liquid characteristics/properties. These studies were aimed at modeling the amount of liquid infiltration of the spreading liquid into the sub-surface area. The infiltration models developed were then coupled with a spreading model to determine the impacts of permeable surfaces. Keller et al. [2005] also noted that capillary effects could not be neglected when determining infiltration into a permeable surface. That is to say, capillary suction within a substrate would influence absorption in addition to the hydrostatic pressure effect, which adds further complexity to this type of problem. The most notable difference between liquid spread on a permeable surface and a non-permeable surface is that it is possible for the entire liquid volume to be absorbed into the subsurface when a permeable surface is concerned. This means that liquid spread on permeable surfaces tends to be much more transient than on impermeable surface. Therefore, it is more difficult to determine an accurate spill thickness on a permeable surface.

2.1.2 Surface Topography

Surface topography is also a key parameter when considering the spread of a liquid. The topography characteristics of a surface include levelness, roughness, and uniformity. Each of these characteristics will affect the extent to which a liquid spreads across a surface thus the final area and depth of the spill. Surface roughness can be described as a measure of the texture of a surface. The measure of roughness takes into account the amount of vertical variations of a surface from its average location. If these variations are large and plenty, the surface can be considered rough, else it would be considered smooth. The main difference between rough surfaces and smooth ones is that for the same size area, a rough surface will tend to have more microscopic surface area. This is due to the increased number of small peaks and valleys on the surface. This will play an important role in liquid spills because, due to the increase in surface area, a rough surface will tend to be more absorptive. Also, the peaks and valleys in a rough surface tend to act like cups that hold the liquid spill. This means that the spill thickness determined on a rough surface would not be similar to that of a smooth surface because the liquid would be more readily absorbed and held below the top plane of the surface. Uniformity can be thought of as how overall flat, i.e. without macroscopic peaks and valleys, a surface is. This would impact a spill because liquids tend to pool in low spots of a surface or area, thus making the spill thickness on the surface non-uniform. Non- levelness in a substrate presents much the same problem as a non-uniform surface in that liquids tend to move towards low spots, or towards the bottom of an inclined (non-level) surface. Spills on non-level substrates were addressed by Simmons et al. [2004]. This study showed that even small inclines on the order of 1^{o} can over time affect the behavior of

a liquid spill. However, the spill creeping introduced by a small incline would tend to be slow. Obviously, it can be seen that for a larger incline there will be a larger impact on spill behavior.

2.1.3 Evaporation

Evaporation during liquid spread is another complicating factor when considering volatile liquids such as some hydrocarbon fuels. In most environments, aside from extreme temperature conditions where evaporation can be rapid, the majority of a liquid spill will remain as liquid during the time it takes for the liquid to reach an equilibrium state. A study conducted by Okamoto et al. [2009] measured the evaporation rates for gasoline in a 0.1 m^2 pan with various depths (0.1-0.3 cm). It took approximately two and six hours for 70% of the gasoline to evaporate for the 0.1 cm and 0.3 cm depths, respectively. This is much longer than a typical spill time, which is on the order of minutes rather than hours. DeHaan [1999] found that evaporation of flammable liquid pools also exhibited a strong dependence on ambient temperature. It was noted by DeHaan [1999] that compared to pools at 20^{o}C, evaporation rates decreased by about 50% for pools initially at 5^{o}C and increased by about 50% for pools initially at 35^{o}C. Examination of both of these sources suggests that for short time scales, under ambient temperature of approximately 20^{o}C, and in a quiescent environment, that the amount of evaporation of a volatile fuel is small.

2.1.4 Liquid Fuel Spill Depths

Few studies have been conducted that were aimed at characterizing the depth of an unconfined liquid fuel spill. Modak [1981] spilled high flash-point hydrocarbon oils on concrete, epoxy coated concrete, and steel substrates. In this study, Modak [1981] found unconfined spill depths of approximately 0.1 cm. In addition, this work showed that the spill depth determined was independent of volume on an impermeable surface. Putorti et al. [2001] studied gasoline and kerosene spills on residential flooring including wood and vinyl materials. Putorti et al. [2001] found similar results measuring spill thicknesses of less than 0.2 cm. The findings of Gottuk, et al. [2001] and Chambers [1977] also found spill thicknesses that fall into the range of less than 0.1 or 0.2 cm for hydrocarbon spills on concrete substrates. Despite the limited nature of the data available for liquid fuel spills, all of the data points to fuel spill thicknesses less than 0.2 cm on various types of substrates.

The dynamics of liquid spills for both flammable and non-flammable liquids have been reviewed. Further discussion will focus on the burning rates of flammable liquids in various configurations.

2.2 Burning Rate of Liquid Fuels

2.2.1 Pool Fire Burning Rate

When investigating the burning rate of a liquid fuel, most of the literature focuses on the steady state burning of liquid fuels in a pool configuration. The reason for this focus is that pool fires are easily repeatable and widely relevant fire scenarios. The foundation for most of this work can be found in Blinov & Khudyakov [1961].

This classical paper provides a wealth of information on the burning rate of various sized liquid fuel pools. Blinov & Khudyakov [1961], a US Army translation of work by Blinov & Khudyakov performed before 1958, found the regression rate (burning rate) for a liquid fuel pool for pan diameters from 0.0037m to 22.9m. A plot of this can be seen in Figure 2-3. This plot shows similar burning rate behavior of liquid pool fires for a variety of common fuels, as well as the flame height to pan diameter ratios. Further analysis of this work by Hottel [1958] divided the burning rate into two primary modes: convectively driven and radiatively driven burning. The convectively dominated regime was further split into laminar and turbulent convection.

A relationship describing the mass burning rate for radiatively driven pool burning was first developed by Zabetakis et al. [1961] and is presented in equation (2):

$$\dot{m}_f'' = \dot{m}_{max}'' (1 - e^{-k\beta D}) \tag{2}$$

where D is the pool diameter, κβ is an empirical constant, and $\dot{m}_{max}''$ is the empirically determined mass burning rate for an infinite-diameter pool. Babrauskas [1983] summarized the maximum burning rates found for various fuels and their κβ values. Equation (2) is generally used to determine burning rates for liquid pool fires in the radiatively dominated regime, where diameters are typically larger than 0.2m [SFPE, 2002]. The turbulent convectively dominated burning rate is approximately constant and is accounted for in equation (10). Burning rate for a liquid pool in the convectively dominated regime can be determined through analytical methods presented in Quintiere [2006]. This method is outlined in Appendix A and shows a burning rate proportional to the diameter to the -1/4 power.

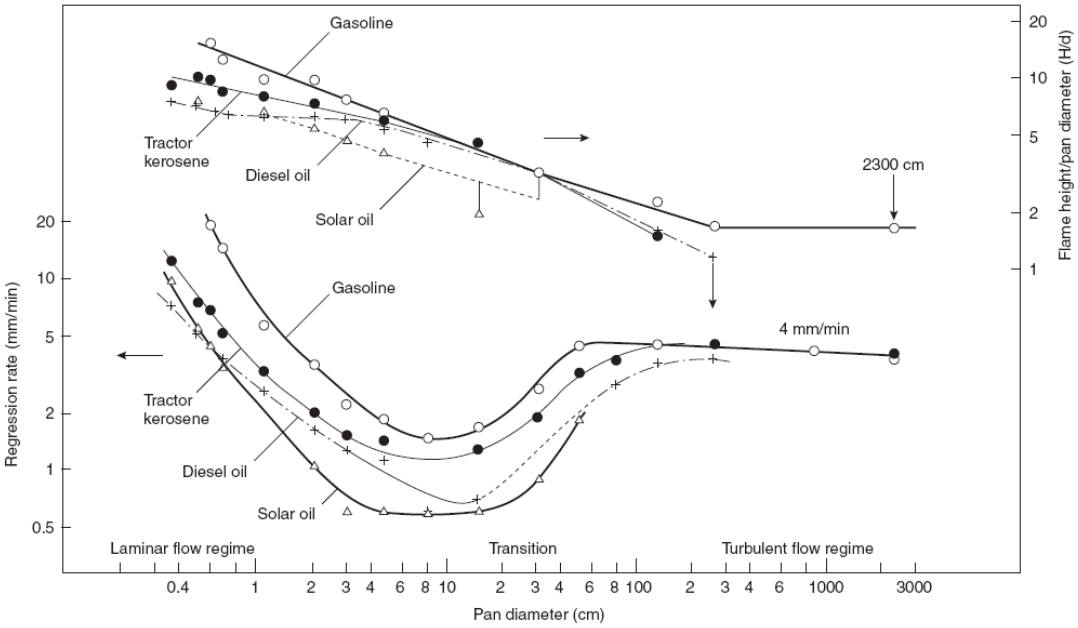

Figure 2-3 - Regression Rate & Flame Height from [Blinov & Khudyakov, 1961]

It should be noted that the data presented in Figure 2-3 , data in Babrauskas [1983], and the data used to determine equation (2) were steady-state values of burning rate. These were determined using deep liquid pools or continuously fed liquid pools in steel or concrete pans. These methods allowed for the large quantities of fuel and time required for a pool fire to reach steady state. As a result, the use of these data sets should be limited to scenarios where a deep pool is concerned.

Some studies have been conducted on unsteady pool fire burning rates. Research by Garo et al. [2007] conducted liquid pool fires of varying diameter (15-300 cm) and initial fuel depth (2-100 mm) found that the burning rate of fuel on top of water varied based on the initial depth of fuel. It was found that the burning rate tended to decrease as the depth of fuel decreased. The smallest depth of fuel that was tested in this study was 0.2 cm, a value that is close to the depth of an unconfined liquid fuel spill. Hayasaka [1997] noted that for small 5 cm diameter unsteady pan fires using methanol, gasoline, and kerosene there existed a pre-heating stage where

the fuel is heated from the ambient temperature to the boiling temperature. During this pre-heating stage, the burning rate of gasoline and kerosene in particular were lower than at boiling. This study reveals that lower initial burning rates for unsteady pool fires were due to the heat loss that went into raising the temperature of the fuel and pan used. Exploring the burning behaviors of steady and unsteady liquid pool fires has revealed a great deal of information that will be useful when investigating spill fire burning rates.

2.2.2 Fuel Spill Fire Burning Rate

The few studies that have examined the burning rate of liquid fuel spills have found that the burning rates of liquid spills vary greatly from that of a similar sized pool fire. Gottuk et al. [2001] found that burning rates for spills of JP-5 and JP-8 were approximately 20% of those found in Babrauskas [1983] for steady state pools of comparable diameter. Putorti et al. [2001] obtained a similar decrease in burning rate for gasoline spill fires on wood and vinyl flooring. The current theory for why the burning rate for a liquid spill is vastly different than that of a deep liquid pool is the effect of heat loss to the spill substrate [SFPE, 2002].

The unsteady pool fire results presented in Garo et al. [2007] tend to agree with the above spill fire burning rates for the thin fuel layers tested. A hypothesis provided by Garo et al. [2007] for the differences in burning rate was that the water substrate acted as a heat sink for the fuel layer. This explanation is similar to that presented previously, where the reduction in burning rate is attributed to the substrate acting as a significant heat sink for the thin layers of fuel.

Several studies have been conducted that address continuously fed spill fires including that of Cline et al. [1983]. This study was designed to model a continuous spill fire originating from a large fuel tank with a hole in it. Experiments involved burning small scale continuously fed gasoline fires on a flat steel plate. Cline et al. [1983] found that in order to correlate their spill fire model with experiments, the regression rate used in the model had to be varied significantly from published pool fire burning rate values. In addition, a lower initial burning rate was found during experiments, which was attributed to early heat losses to the substrate. Croce et al. [1986] modeled an unconfined continuously fed spill fire by equating the discharge rate into the pool to the steady state pool burning rate. This model would allow one to determine the steady state pool diameter knowing the discharge rate. Croce et al. [1986] assumed that for an instantaneous fuel spill, the pool radius would continue to grow until all of the fuel was consumed. The burning rate used in this model was again the steady state pool burning rate as a function of diameter. None of these spill fire models account for heat losses that are seen prior to steady-state burning for smaller pool fires.

2.2.3 Liquid Spill Ignition

Some thought must be given as to whether a liquid fuel spill is able to be ignited and under what conditions this is possible. For fuels at temperatures greater than their flashpoint, flame spread requires only an ignition source. A relevant factor affecting the ability to have ignition in the case of a fuel above its flash-point is the thickness of the fuel layer. Modak [1981] conducted tests to determine the ignitability

of thin spills of high flashpoint liquids. It was found that for a constant heat flux, the temperature of liquid fuel spills increase more rapidly for thicker spills. This was due to the increased heat losses to the substrate for thinner spills.

3 Liquid Spill Tests on Concrete

3.1 Experimental Background

The purpose of the liquid spill experiments was to determine the equilibrium spill thickness, δ, for a certain liquid. According to Modak [1981], Simmons et al. [2004], and Bradley [2002], the equilibrium spill thickness is a property of a liquid and substrate combination and is independent of spill volume. Knowing the characteristic spill thickness for a liquid/substrate combination, one would be able to calculate the spill area (A) if the volume (V) of the liquid spilled is known using the following equation (3):

$$A = V/\delta \tag{3}$$

Equation (3) assumes that the spill thickness is uniform over the spill area, which does not take into account the curved edges of the spill as can be seen in Figure 2-2. This could have an impact on the measured thickness of a very small droplet when using this method. In addition, surface topography impacts, discussed previously are not taken into account in this calculation.

The spill area will become very important when examining the burning rate of liquid fuel spills. Although the primary focus of this report is that of liquid fuel spill fires, it is necessary to explore non-flammable liquid spills before flammable fuels. The reason for this is that the dynamics of liquid spills should be explored and

understood before moving on to volatile fuels, which could present a safety hazard. In addition, the use of the non-flammable liquids provides additional liquid spill data and an alternate method for determining spill thickness, using liquids with similar properties. Modak [1981] and Simmons et al. [2004] both determined that the primary liquid properties governing spill layer thickness are surface tension and contact angle. If a non-flammable liquid were chosen that had similar properties as a liquid fuel in question, one could make the assumption that these two liquids would have similar spill behavior and thickness. The purpose of this testing is to address this assumption. Only the non-flammable liquid spill results will be discussed in this section, the flammable liquid spill results will be covered later.

3.2 Liquid Spill Experiments

A total of five liquids were used in testing: three non-flammable liquids and two flammable liquids. The two commonly available liquid fuels used for testing were 87 Octane Automotive Gasoline and SLX Klean Strip Denatured Alcohol. Denatured alcohol is ethanol with an additive that makes the liquid not fit for human consumption. The non-flammable liquid choice was based on choosing liquids with surface tensions that bounded those of the liquid fuels. These three liquids were 3% and 6% concentration by volume Aqueous Film Forming Foam (AFFF) solutions in addition to tap water. A 6%AFFF solution was used in addition to a 3%AFFF solution to examine effects of density changes on spill depth, while keeping surface tension constant. Table 3-1 shows the surface tension, density, and contact angle values for each of the liquids used in the spill thickness testing, from various sources.

Flammable liquid properties are included for comparison to non-flammable liquids. The substrate that was used for contact angle testing was smooth concrete, which will be described in detail later.

Table 3-1 - Liquid Properties

	Surface Tension (N/m)	Density[a] (kg/m^3)	Contact Angle (°)
Water	0.0720[b]	999	65 - 125[b]
3% AFFF	0.0172[c]	990	14.2[c]
6% AFFF	0.0172[d]	980	14.2[d]
Gasoline	0.0219[c]	790	19.7[c]
Denatured Alcohol	0.0223[c]	742	19.7[d]

a- Measured
b- Literature Values
c- Experimentally Determined
d- Assumed

With the exception of water, both the surface tension and contact angle values for all liquids were determined via analytical testing. The surface tension of water is widely found to be 0.072 N/m [Simmons et al., 2004]. However, the contact angle for water on concrete can be found to have various values including 65 degrees [Rousseau, 1993], 110 degrees [Kligys et al., 2007], and 125 degrees [Simmons et al., 2005], depending on the concrete used. Therefore an average of the high and low values was assumed (85 degrees). For all liquids other than water, the liquid/substrate properties that were determined by analytical testing shown in Table 3-1 were measured by Augustine Scientific Laboratories in Newbury, OH. Some assumptions were made in order to optimize the amount of analytical testing that needed to be conducted. The surface tension of 6%AFFF was not determined analytically because

per the manufacturer's specifications, it is equal to that of 3%AFFF. Contact angle testing was conducted for 3%AFFF and gasoline on smooth concrete while denatured alcohol and 6%AFFF were omitted due to limited resources. Due to the similarity in liquid properties (density and surface tension), the contact angles of denatured alcohol and 6%AFFF were assumed to be equal to those of gasoline and 3%AFFF, respectively. This assumption is reasonable because if one looks at equation (1), Young's Law, and how the properties of the fuel and substrate impact contact angle, the only property that is different for different fuels with similar surface tensions is the liquid-solid interfacial tension. It is a safe assumption that the liquid-solid interfacial tension does not vary significantly between liquids with similar properties.

The surface tensions of the three liquids tested (3%AFFF, gasoline, and denatured Alcohol) were measured in triplicate using Wilhelmy plate measurements on a Kruss Tensiometer K100 at room temperature (22^{o}C) by Augustine Scientific. Densities were calculated by dividing a measured weight of liquid by the known volume of that liquid. Contact angles were measured by Augustine Scientific using the dynamic sessile drop method. Values for initial contact angle are presented and were averaged over 5 tests. The contact angle was determined through examination of video images, such as the one in Figure 3-1.

Figure 3-1 - Example contact test photo for 3%AFFF drop on concrete

3.2.1 Experimental Design

All liquid spill tests were conducted at the Alcohol Tobacco and Firearms (ATF) Fire Research Laboratory (FRL) at the National Laboratory Center in Beltsville, MD. The spill and spill fire tests were conducted on a smooth concrete substrate. Concrete was chosen as the testing substrate to represent a common flooring material in residential, commercial, and industrial settings. Also, for the spill fire tests, this substrate allowed repeat testing without the need for repair or replacement. The square concrete pad was 2 m by 2 m and had a smooth finish. The pad was poured 0.05 m deep in a wood frame and finished with a 0.46 m wide aluminum bull-float. Although concrete slabs are typically poured with thicknesses from 0.1-0.2 m, it was assumed that the 0.05 m thickness provided a large enough thermal sink for the durations expected from spill fires (on the order of minutes) and allowed for a more movable pad. The concrete used was Type I, which used a 6.5 bag mix (i.e. 6.5 bags of Portland cement per cubic yard of concrete). This mix was found to be the most common type for concrete pads found in commercial and industrial use. The concrete pad used in testing was poured and finished by a professional contractor and was allowed to cure for a minimum of 28 days before any testing occurred, which is typical practice for concrete construction. Figure 3-2 below shows the smooth texture of the concrete pad that was used. The density of the concrete used was determined by dividing the weight by the volume of a measured sample of the cured concrete. The density of the concrete used was found to be 2224 kg/m^3.

Figure 3-2 - Smooth texture of concrete pad used in testing

The amount of liquid to be spilled was based on the expected diameter of the spill. It was intended to achieve spill sizes ranging from approximately 2.5 cm to 1.0 m in diameter. Using previous spill thickness results from the literature, it was determined that the liquid volumes should range from 0.2 ml to 450 ml in volume. The ten volumes used were, in ml, 0.2, 6.65, 25, 80, 125, 200, 240, 290, 350, and 450. Tests for each volume were run in duplicate for each liquid. This resulted in 59 spill tests total, with one volume excluded for one liquid.

A spill apparatus was constructed to provide a reproducible method of spilling the liquids onto the concrete. This method allowed the spill height and spill outlet diameter to be constant between tests. Two versions of this spill apparatus were constructed: one for 0.2 and 6.65 ml spills and the other for 25-450 ml spills. The reason for this was that the 0.2 and 6.65 ml spills were only able to be accurately measured and spilled out of a 25 ml pipette with 0.1 ml increments, while the larger spill volumes could be spilled through a funnel using a larger graduated cylinder. The spill apparatuses were constructed using a metal ring-stand with a horizontal bar and counterweight. A clamp at the end of the horizontal bar held either a pipette or a

funnel, for 0.2 and 6.65 ml or 25-450 ml spills, respectively. Figure 3-3 shows the test apparatus with the pipette in the clamp and the funnel used for the larger spills.

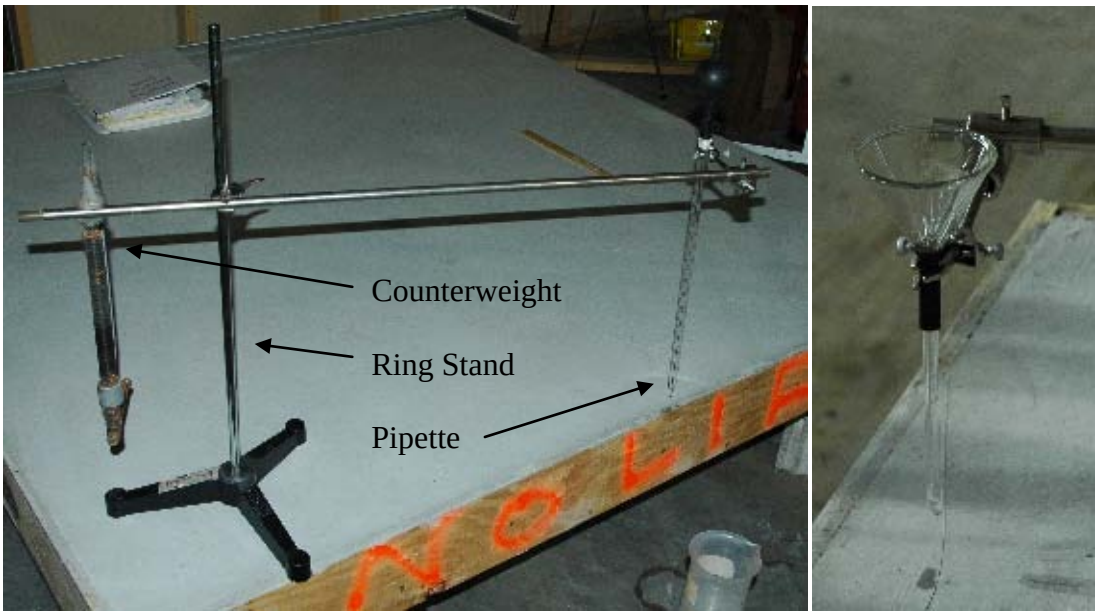

Figure 3-3 - Spill apparatus with pipette (left) and funnel (right)

The outlets of the pipette and the glass funnel were placed at 4 cm above the concrete pad to reduce any liquid splashing outside of the spill.

3.2.2 Experimental Procedure

The non-flammable liquids used, other than water, were a Buckeye 3 percent aqueous film forming foam (3% AFFF) solution and Buckeye 6 percent aqueous film forming foam (6% AFFF) solution. These solutions were mixed by test personnel per manufacturer requirements. The 3%AFFF solution consisted of mixing 150 ml of 3%AFFF foam concentrate with 4.85 liters of tap water yielding a total batch volume of 5 liters of solution. The 6%AFFF solution consisted of mixing 300 ml of 6%AFFF foam concentrate with 4.7 liters of tap water yielding a total batch volume of 5

liters of solution. The mixed solutions were used for testing within one week of mixing. This was not required; however it was done to ensure that no changes occurred within the batch as a result of degradation. The water used separately and in the AFFF solutions was tap water that was collected and allowed to reach the ambient temperature of around 20^{o}C before mixing or spilling.

The concrete pad was placed in an indoor environment in still air. The ambient temperature ranged from 20^{o}C to 26^{o}C. The spill apparatus was placed on the pad with the spout of the funnel or pipette at the center of the intended spill area. The location of spilling changed from test to test. This was done for two reasons: to reduce the effects of localized imperfections in the concrete pad on spill thickness results and to facilitate testing on a section of the pad that was dry before the previously tested area was dry. The spout of the discharge device (funnel or pipette) was then adjusted to 4 cm above the concrete pad. All liquid volumes were measured with graduated cylinders with increments of 5 ml, with the exception of the 0.2 ml and 6.65 ml volumes that were measured using the 25 ml pipette with 0.1 ml increments. The liquid volume was then spilled on the concrete at a constant rate dictated by the discharge device. The spills discharged through the funnel were poured into the funnel such that the liquid level was near the top of the funnel. The spill time was almost instantaneous for the smallest volumes and approached 30 seconds for larger volumes. Because the time to spill a volume was typically much less than the spreading time, this method of spilling was deemed quasi-instantaneous.

The spill was allowed to spread until it visibly ceased, at which time an equilibrium state was assumed to have been reached. For small volumes, this

occurred very quickly, on the order of a few seconds and for the larger spill volume, it took up to approximately 3 minutes. It was not possible to set a spreading time that was constant for all volumes because spreading time is dependent on volume [Putorti et al., 2001]. Also, if too long a time was allowed absorption would tend to have a larger effect.

At the point where equilibrium was determined, several photographs of the spill area was taken from directly above. The camera used in this testing was Nikon D70 digital SLR camera. A ruler placed next to the spill was used for scaling. Some examples of typical spill photos with rulers placed next to the spill area can be seen in Figure 3-4.

Figure 3-4 - Photos: 6.65 ml(right) & 125 ml(left) 3%AFFF spill, ruler for scale

After all necessary photographs were taken; the spill was cleaned off of the pad using cloth towels. The pad was rinsed with water in order to remove any residue from the spilled liquid and then was dried using forced air convection provided by industrial fans blowing over the concrete pad surface. For smaller volume spills, the spill apparatus could be repositioned in order to run another test on a dry section of concrete before the entire pad was completely dry. For larger tests, where the spill

could have spread onto a previously wet area, the entire pad was allowed to dry before another test was run. The pad was deemed dry when no surface wetness was visible.

3.2.3 Spill Area Calculation

The liquid spill areas were determined from the test photographs using a National Institute of Health image analysis program called ImageJ. ImageJ is a very sophisticated program that, among other functions, can calculate the area of objects in a photograph. ImageJ uses a pixel counting algorithm to determine area of an object within a boundary. The process begins by opening each photograph with ImageJ. The calibration length was then selected as a 10 cm length of the ruler in the picture and the image scale was set. Then the spill area was outlined carefully using the tracing tool. ImageJ then calculated the traced area of the spill in cm^2. The spill volume was then divided by this area in order to find the spill thickness based on equation (7). This assumed that the spill thickness was constant over the entire spill area. A screenshot of ImageJ is shown in Figure 3-5 illustrating the spill tracing method. This method of area calculation was calibrated with photographs of circular objects with known areas. It was found that the method determined the area of the calibration images within 5% of their known area. One point to note is that this method measures the perceived spill area, that is to say the perimeter traced is where the liquid wets the surface. It is possible that the visible area differs slightly from the area on which the spill rests due to capillary effects along the edge.

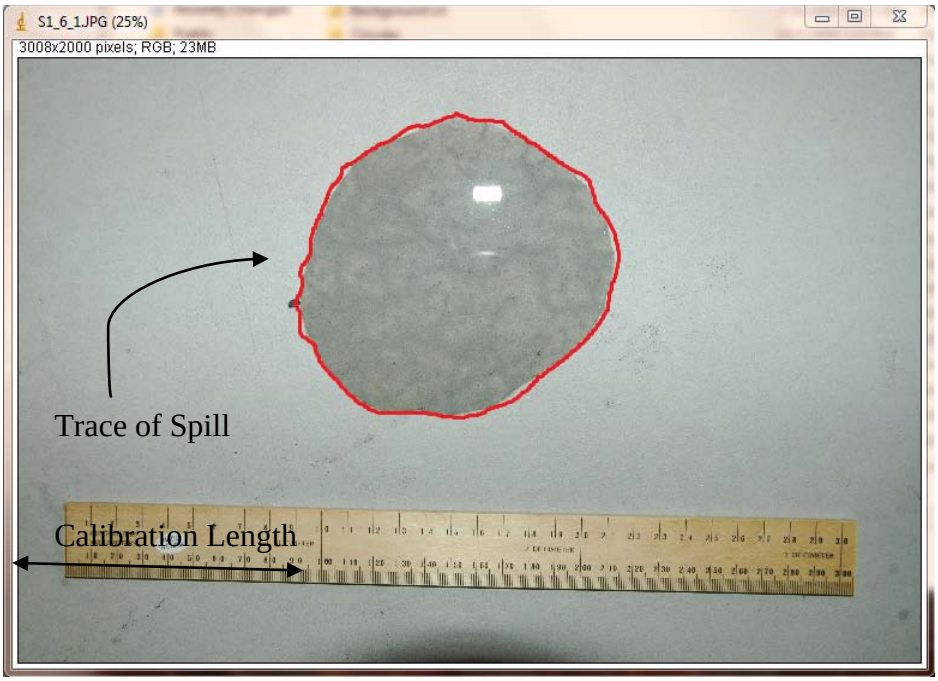

Figure 3-5 - Example of ImageJ Processing

3.2.4 Results

A total of fifty-nine liquid spill tests were conducted with three liquids. All but one liquid volume had duplicate tests. The average spill thicknesses for each volume and type of liquid are presented in Table 3-2 along with the averages and standard deviations for each liquid. These values are also plotted in Figure 3-7. A complete set of spill area and spill depth data for all tests can be seen in Table C-1 through Table C-3. For both the 3%AFFF and 6%AFFF, all spill thicknesses were less than 0.1 cm, which is consistent with the spill thicknesses found in the literature for similar liquids. All water spill tests were found to have spill thicknesses that were less than 0.2 cm, similar to results found in the literature [Simmons et al., 2004]. Repeatability between duplicate test results was generally good. However, for some spill volumes, spill thickness differences between duplicate tests were up to 50%, in

the rarest cases. This can be seen in Table C-1 through Table C-3. From the results seen in Figure 3-7, it can be inferred that spill thickness is a function of spill volume because the spill thickness tends to decrease as very small volumes are approached. This behavior is possibly due to the method of area measurement, which captured the visibly wet area, not necessarily the area that the spill was atop. Capillary action tends to pull some liquid along the perimeter outwards through the pores at the surface of the substrate, thus creating a larger perceived spill area. This effect would become less important as spill volumes increase because the length scale of the capillary action becomes smaller when compared to diameters of the larger volumes.

Table 3-2 - Average spill depths for liquid spills

Volume	Average Spill Depth (cm)		
(ml)	Water	3%AFFF	6%AFFF
0.2	0.095	0.017	0.022
6.65	0.152	0.031	0.033
25	0.214	0.038	0.045
80	0.246	0.044	0.046
125	0.224	0.054	0.054
200	0.251	0.066	0.066
240	0.230	0.058	0.059
290	0.267	0.089	0.056
350	0.243	0.082	0.064
450	0.285	0.065	0.067
Average	0.221	0.054	0.051
Std. Dev	0.057	0.022	0.015

For whatever reason, spill depths found in these experiments seem to have an exponential behavior, resulting in large standard deviations seen in Table 3-2. An exponential fit was used in the following form to represent the spill thicknesses' dependence on volume seen in the experiments:

$$\delta = \delta_{\text{inf}}(1 - \mathrm{e}^{-\varepsilon V}) \quad (4)$$

where δ_{inf} (cm) is the asymptotic spill depth for an infinite volume of liquid and ε (ml^{-1}) is the exponential spill depth factor. The exponential fits can be seen along with experimental data in Figure 3-7. Table 3-3 shows the asymptotic spill depths and exponential spill depth factors for the non-flammable liquids.

Table 3-3 - Asymptotic spill depths and exponential spill depth factors for non-flammable liquids

	Water	3%AFFF	6%AFFF
ε	0.1	0.05	0.05
δ_{inf}	0.250	0.069	0.061

The impact of surface tension on the spill thickness can also be seen from Figure 3-7. Water having a surface tension of 0.072 N/m produces a spill thickness significantly larger than that of 3%AFFF and 6%AFFF with surface tensions of 0.0172N/m. This has the propensity to verify the theory that on the same surface, larger surface tensions produce larger spill thicknesses. The impact of liquid density cannot be established by these results as the small difference in density between the 3%AFFF and 6%AFFF solutions did not seem to produce any significant change in spill thickness. However, the flammable liquid spill results will likely be a better gauge for the impact of liquid density on spill thickness as their densities are significantly different than the other liquids while their surface tensions are similar to 3% and 6% AFFF. Some typical spill photos are shown for 350 ml spill volumes for the various non-flammable liquids in Figure 3-6. These show the some of the different shapes and spill sizes that were obtained during testing for a given volume.

Figure 3-6 - Typical 350 ml spill photos: water (left), 3%AFFF (middle), & 6%AFFF (right). Ruler used for scale.

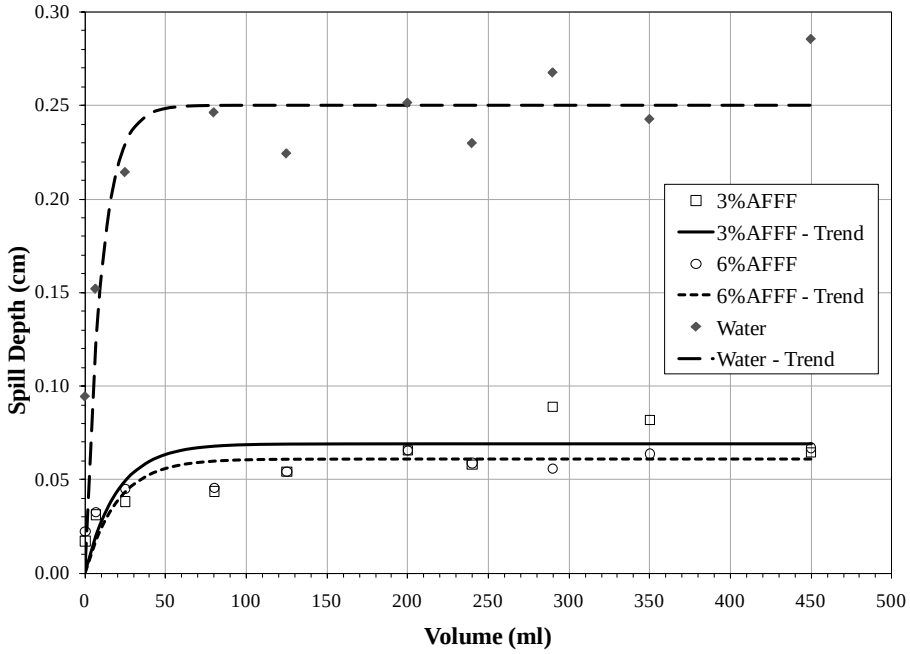

Figure 3-7 - Spill thickness vs. volume for liquid spills, with exponential fits

Even though these spill tests generally show that for large volumes a liquid spill thickness on a certain substrate is independent of spill volume, there is still a significant amount of scatter in the data. There are a few possible reasons for this that include, but are not limited to, error in area calculation, error in volume measurement, unpredictability in spill shape, and the effect of imperfections in the substrate. The first two errors will tend to be small; however, the latter two could be significant and should be examined further. A plot of the area of the spill as a function of spill

volume for all tests for the three non-flammable liquids can be seen in Figure 3-8. It can be seen that the spill area increases in an almost linear fashion as the spill volume increases. The slope of a linear trend line for these liquids will yield a particular spill area per unit volume for each liquid: 14.9, 16.1, and 3.87 cm^2/ml for 3%AFFF, 6%AFFF, and water, respectively.

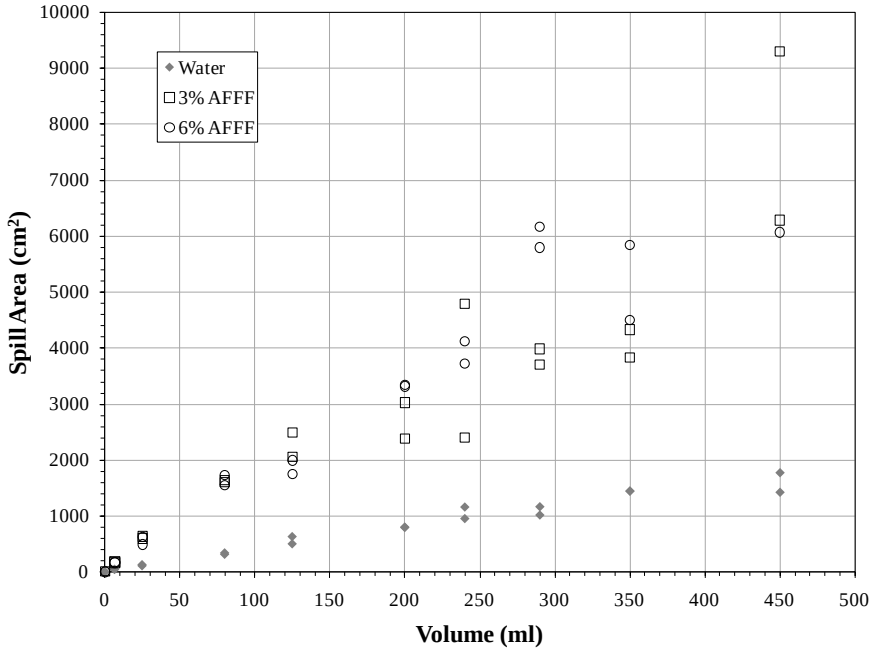

Figure 3-8 - Spill area versus volume plot for all non-flammable liquid tests

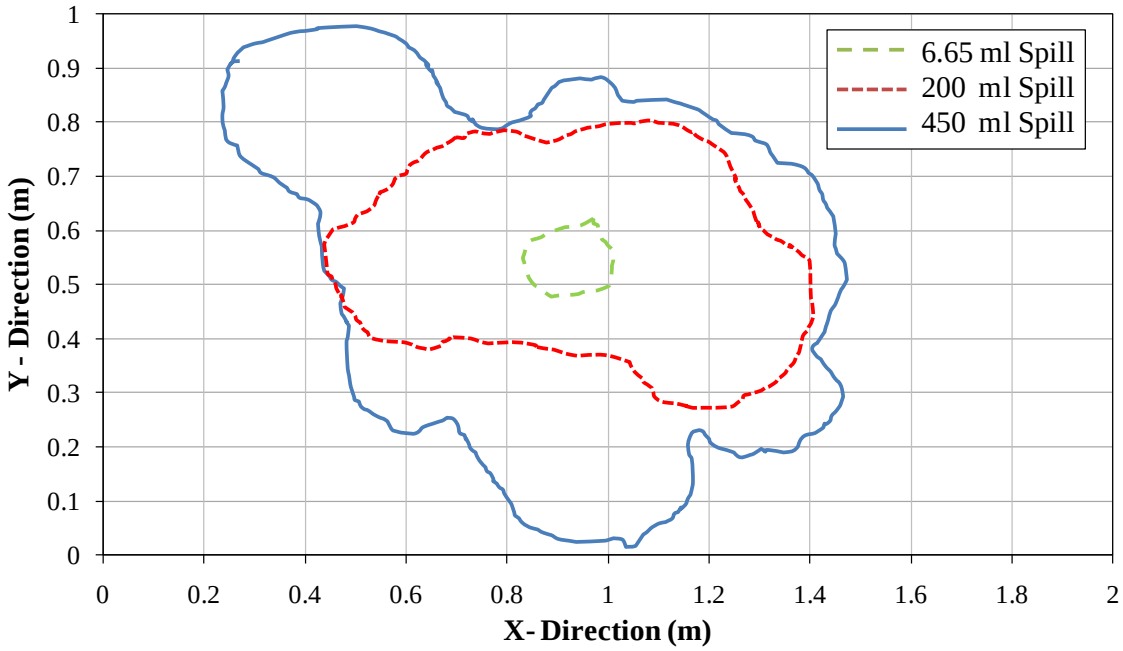

Figure 3-9 - Nested spill outlines for some 3%AFFF spills

Figure 3-9 shows the outlines of three 3%AFFF spills, of various volumes on an arbitrarily located grid representing the concrete substrate. These were not spilled atop the same area, but the outlines are nested in order to visualize the spills and to compare to each other. An interesting thing to note is that the spills are not similarly shaped. The 450 ml spill has various “fingers” protruding from the central spill area, the 200 ml spill is close to a bent oval, and the 6.65 ml spill is ovular in shape. The significance of these shapes is to show that for practical purposes, liquid spills can have a variety of different shapes not necessarily circular. Often, the topography of the substrate can influence how and where the liquid spreads. That being said, it is possible that some differences in the spill thickness data could have arisen from the random nature of the spill shape produced by the imperfect substrate. It was observed, however that for spills located on the same area, spill shape tended to be similar. Therefore, it would have been possible to reduce uncertainty between duplicate tests

by spilling over the same area. However, if this method was used, the effects of surface topography might not have been recognized even though they are present.

4 Liquid Spill Fires on Concrete

4.1 Experimental Background

The purpose of the liquid spill fire tests on concrete was to determine the spill size and burning rate of liquid fuel spills. These tests build upon the results from previous tests with non-flammable liquids and follow much of the same methodology. As stated previously, the two liquid fuels chosen were denatured alcohol (ethanol) and automotive gasoline. The surface tension and contact angle values for these fuels can be found in Table 3-1 and were determined by analytical testing, described in Section 3.1. These liquid fuels were chosen due to their widespread availability to the public in various quantities and because the burning dynamics of the two fuels tend to vary significantly for pool fires. All flammable liquids were bought in bulk quantities from the same distributor at the same time in order to reduce the chance of variations in properties. The gasoline used was ‘regular’, unleaded gasoline purchased from a local fuel distributor with an octane rating of 87. The denatured alcohol, manufactured by W.M. Barr Company, and distributed under the product name Klean-Strip SLX Denatured Alcohol was purchased from a local hardware store. The spill fire test results that will be discussed include fuel spill thicknesses, average burning rates, and some transient diameter measurements.

4.1.1 Experimental Design

All liquid spill fire tests were conducted at the Alcohol Tobacco and Firearms (ATF) Fire Research Laboratory (FRL) at the National Laboratory Center in Beltsvile, MD. In order to have continuity between the liquid spill fire tests and the liquid spill tests, much of the same procedures for testing were shared. The same spill apparatus shown in Figure 3-3 was used to spill the liquids. The concrete substrate described in section 3.1 was used for liquid spill fire tests. Due to the complexity of the liquid spill fires, a more involved test setup was required. A flame height indicator with vertical marker spacing of 0.25 m and marker length 0.25 m was used as a length scale for determining the flame diameter and flame height. The flame height indicator was placed along the centerline of the initial spill location. In addition, a Sony digital video camcorder was used to record video for each of the tests. This camera was placed along the center axis of the concrete pad with full view of the flame height indicator and the entire concrete pad. A schematic of the test setup can be seen in Figure 4-1.

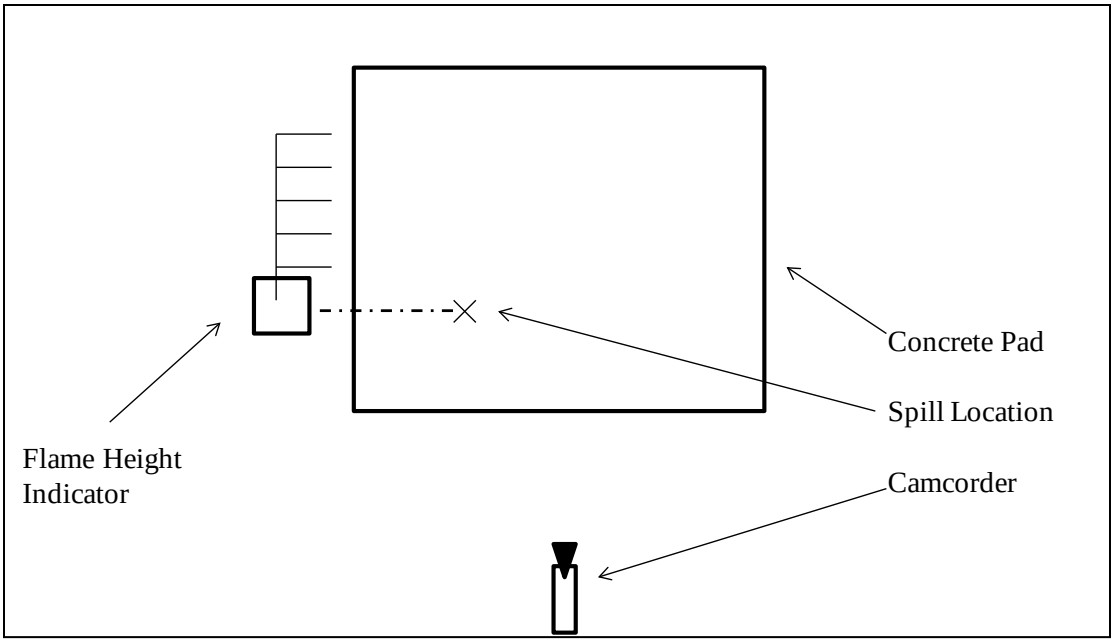

Figure 4-1 - Schematic of spill fire test setup with arbitrary spill location

The mass of all fuel quantities was measured using an Ohaus Explorer Model E1K210 load cell with 12 kg capacity and 0.1 g resolution. The mass of the 0.2 ml spills were calculated from the density of the liquid because the weight of the liquid was approximately equal to the resolution of the load cell.

4.1.2 Experimental Procedure

The flammable liquids used in testing were gasoline and denatured alcohol. These fuels were kept indoors and at ambient temperature throughout the testing period. Ambient temperatures ranged from 20^{o}C to 26^{o}C during testing. The concrete pad was set up in an indoor environment without significant ambient wind. The spill apparatus was placed on the pad with the spout of the funnel or pipette at the center of the intended spill area. The location of spilling changed from test to test. This was done for two reasons: to reduce the effects of localized imperfections in the concrete

pad on spill dynamics and to facilitate testing on a cool and dry section of the pad before the previously used spill fire area had cooled. The spout of the discharge device (funnel or pipette) was then adjusted to 4cm above the concrete pad, with the spout at the intended spill center. The flame height indicator was aligned with the approximate center of the intended spill area. All liquid volumes were measured with graduated cylinders with increments of 5 ml, with the exception of the 0.2 ml and 6.65 ml volumes that were measured using the 25 ml pipette with 0.1 ml increments. The mass of the liquid spilled was recorded, except for the 0.2 ml volumes, which was calculated later.

The liquid volume was then spilled on the concrete at a constant rate dictated by the discharge device. The spills discharged through the funnel were poured into the funnel such that the liquid level was near the top of the funnel. The spill time was almost instantaneous for smaller volumes and approached 30 seconds for larger volumes. Because the time to spill a volume was typically much less than the spreading time, this method of spilling was deemed quasi-instantaneous.

The spill was allowed to spread until it visibly ceased, at which time an equilibrium state was reached. For small volumes, this occurred very quickly, on the order of a few seconds and for the larger spill volume, it took up to approximately 3 minutes. It was not possible to set a spreading time that was constant for all volumes because spreading time is dependent on volume, [Putorti et al., 2001]. Also, if too long a time was allowed the effects of absorption and evaporation would become larger. At the point where equilibrium was determined, several photographs of the equilibrium spill area were taken from directly above. The camera used in this testing

was Nikon D70 digital SLR camera. A ruler placed next to the spill was used for scaling. Some typical spill photos can be seen in Figure 4-2. At this point, the video camera recording was started.

Figure 4-2 - Typical fuel spill photos: 125 ml gasoline (left) and 240 ml denatured alcohol (right)

After all necessary photographs were taken, the ruler was removed from the concrete pad and the photographer ignited the liquid spill with a propane torch from a safe distance. Upon ignition, a timer was started to measure the burning duration. Periodically during the test, photographs were taken of the fire. The time to extinguishment was established when the majority of the spill fire had extinguished on the concrete surface. This measurement was somewhat arbitrary; however, care was taken to determine extinguishment times under similar conditions. Video footage was terminated when no flaming remained on the concrete surface.

After extinguishment, the pad was rinsed with water and scrubbed with a cotton towel in order to remove any residue from the burned liquid. The pad was then cooled and dried using forced air convection provided by industrial fans blowing over the surface. For smaller volume spills, the spill apparatus could be repositioned in order to run another test on a cool and dry section of concrete before the entire pad

was completely cool and dry. For larger tests, where the spill could have spread onto a recently tested area, the entire pad was allowed to cool and dry before another test was run. The pad was deemed cool when the surface where the previous spill fire occurred was cool to the touch. This method was used versus thermocouple measurement of surface temperature because of the difficulty of determining the average surface temperature over the spill location, which was often difficult to distinguish after the test had been conducted. Time between tests was approximately 30 minutes.

4.1.3 Spill Fire Video Analysis

Post testing analysis was conducted on the spill fire videos in order to determine the diameter and flame length of the fires as a function of time. Flame diameter and length were determined at 5 second intervals from time of ignition until extinguishment or until the diameter and flame length could not be measured. The markers on the flame height indicator were used as a calibration length scales both for the diameter and flame length calculations. The vertical 0.25 m spacing was used as a calibration scale for the flame height and the 0.25 m marker length was used as a calibration scale for the flame diameter. From the test videos, the diameters and flame lengths were measured in pixels and then scaled to meters using the flame height indicator length scales. Flame heights were measured from the base of the center of the spill to the flame tip at the time in question. Often flame lengths are measured as a time averaged value over a period of a test; however this was not possible for spill fires due to their transient nature. Flame diameters were measured as the outside

width of the flame base near the centerline of the spill as seen from the front view of the camcorder. An example of this method can be seen in Figure 4-3.

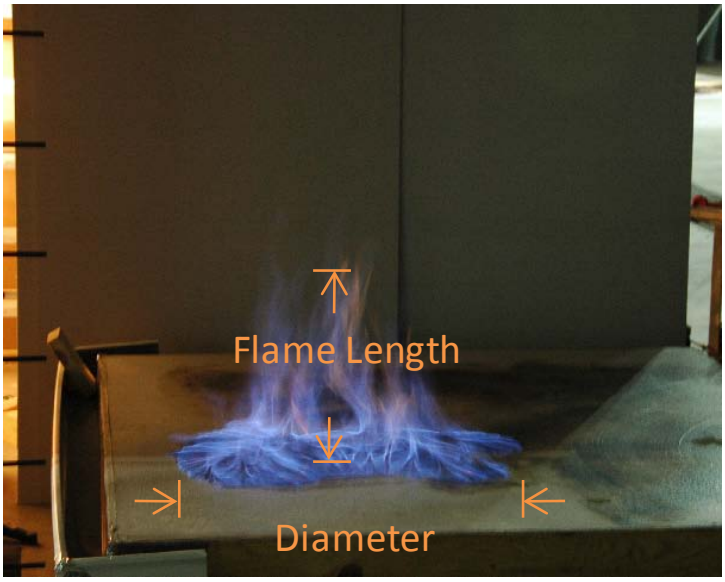

Figure 4-3 - Example of diameter and flame length measurements from video

In some tests, the spill fire split into two fires as seen in Figure 4-4. In the case where one of the flames was significantly larger than the other, the larger diameter would be considered the spill fire diameter. If the two flames were close in size, the diameter measurement was ceased. This was done because at the point where two similar sized flames appear, the diameter measurement becomes much more arbitrary. Due to this difficulty in measurement for some spill fires, there can be significant discrepancies between the times at which diameter and flame length measurements were ceased and extinguishment time for a certain test.

For some of the smaller volume tests, it was very difficult to determine flame height and diameter with the methods used above. Short of making drastic changes to the test setup, the diameter and flame length measurements for the smallest three volumes were not determined.

Figure 4-4 - Sample spill fire photo showing splitting of pool

4.1.4 Results

A total of forty liquid spill tests were conducted with two fuels. Both fuels had duplicate tests for each of the ten different volumes. The average spill thicknesses for each volume and liquid used are presented in Table 4-1 along with the averages and standard deviations for each liquid. These values are also plotted in Figure 4-6. A complete set of flammable liquid spill data can be seen in Table C-4 and Table C-5. The spill thickness was determined using the same method as presented in Section 3.2.3. In general, there was repeatability between duplicate tests. Differences between duplicate tests were typically much less than 30%, but as high as 78% for one case. This case was for the smallest gasoline volume. It was hypothesized that the results in Table 4-1 would show an impact of density on spill thickness, nonetheless it does not seem that this was the case. On the other hand, it is possible that the reason a density impact is not seen between these fuels is because the surface tensions are also different.

Table 4-1 - Average spill depths for flammable liquids

Volume	Average Spill Depth (cm)	
(ml)	Gasoline	Denatured Alcohol
0.2	0.022	0.012
6.65	0.033	0.030
25	0.037	0.038
80	0.045	0.055
125	0.064	0.061
200	0.059	0.061
240	0.080	0.068
290	0.071	0.071
350	0.065	0.069
450	0.064	0.077
Average	0.054	0.054
Std. Dev	0.019	0.021

Tracing of the fuel spill area became tedious when the spill was atop a previously burned area, characterized by a black discoloration of the concrete as seen in Figure 4-5. Still, all fuel spill photos still contained an identifiable spill perimeter that could be traced. The shapes produced by the liquid fuel spills were similar to those found for the non-flammable spills, described in Section 3.2.4 and shown in Figure 3-9.

Figure 4-5 - Photo showing discoloration of the concrete pad from previous tests

Versus spill volume, the average spill thickness data for fuels about the same variation as was seen in the other liquid spills. The coefficients of variation (COV) for gasoline and denatured alcohol were 0.35 and 0.38, while the COVs for 3% AFFF, 6%AFFF, and water were 0.41, 0.29, and 0.25, respectively. The relatively large COV area likely due to the imperfections in the substrate as discussed in Section 3.2.4. Similar to the 3% and 6% AFFF results, all of the fuel spill thicknesses were still under the 0.1 cm depth that is characteristic of a liquid spill. An interesting discovery is that the average spill thicknesses for denatured alcohol and gasoline were essentially equal. This seems reasonable because the liquid properties that impact spill depth (i.e. surface tension and contact angle) are very close for these fuels.

A similar decrease in the spill thickness was seen for the smallest volumes spilled. This accounts for the fact that the spill thicknesses of the larger volumes are above the average value for a particular fuel. For the largest volumes, it can be seen that the spill thicknesses are generally independent of volume. As presented in previous sections, spill thickness dependence on volume seen for smaller volumes is

likely due to substrate effects. An exponential fit was found for the spill thickness data in the same fashion shown in equation (4).The asymptotic spill depths and exponential spill depth factors can be seen in Table 4-2 and the exponential fits are shown with the experimental data in Figure 4-6.

Table 4-2 - Asymptotic spill depths and exponential spill depth factors for flammable liquids

	Gasoline	Denatured Alcohol
ε	0.03	0.02
δ_{inf}	0.067	0.069

Evaporation is mentioned in this discussion to provide a complete outline of possible impacts, but other factors are likely to have had more influence on spill depth. While the effects of evaporation were assumed to be small, it is possible that evaporation could have had a non-negligible impact on calculated spill depths.

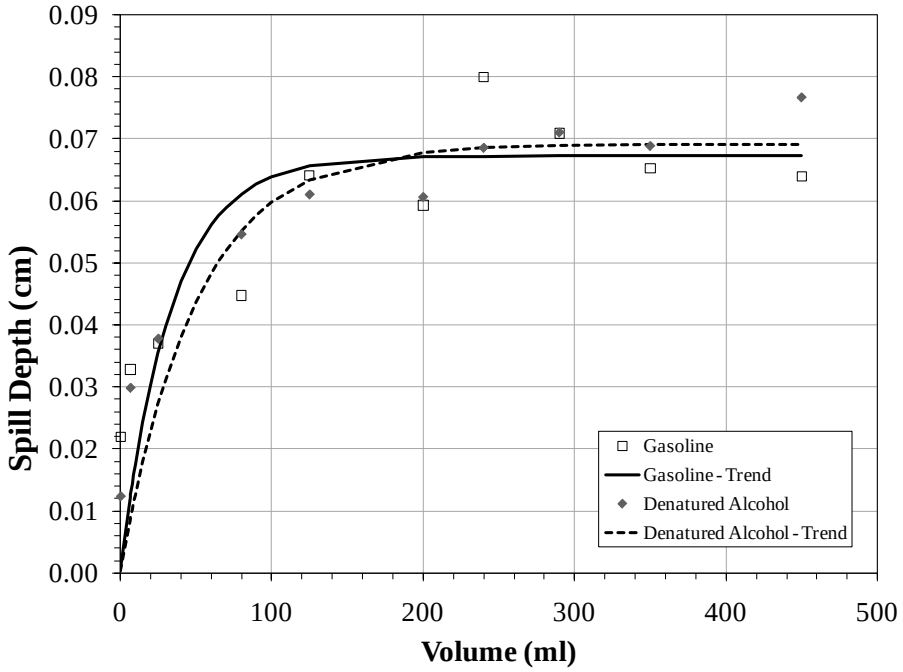

Figure 4-6 - Spill thickness vs. volume for flammable liquid spills and exponential fits

A plot of the area of the spill as a function of spill volume for all tests for the two flammable liquids can be seen in Figure 4-7. It can be seen that the spill area increases in an almost linear fashion as the spill volume increases. The slope of a linear trend line for these liquids will yield a particular spill area per unit volume for each liquid: 10.78 and 10.29 cm^2/ml for gasoline and denatured alcohol, respectively.

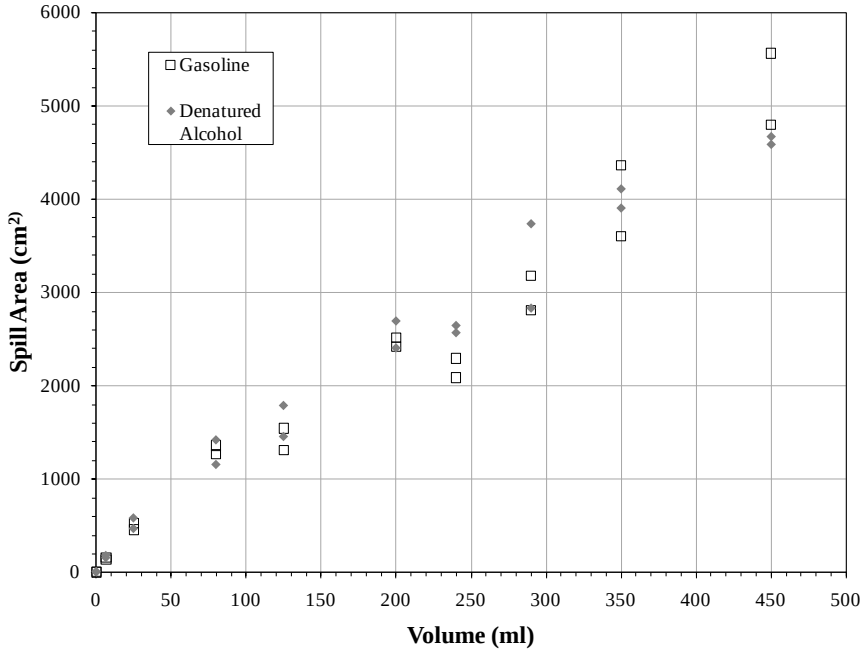

Figure 4-7 - Spill area versus volume plot for all flammable liquid tests

In order to get a coarse estimate of the burning behavior of the liquid spills, average burning rates were determined for each test by dividing the mass of the fuel by the total burning duration. This approximation is somewhat crude, but was used due to the inability to measure burning rate through means such as a load cell with concrete as a substrate. However, this data does provide some insight. The burning rate data can be seen in Figure 4-8 and is summarized with the average burning durations and equivalent initial spill diameters in Table 4-3. Equivalent spill diameters were found assuming a circular spill using the initial fuel spill areas. A complete list of burning rate data can be seen in Table C-4 and Table C-5.

Table 4-3 - Average burning rate, burning duration, and equivalent initial diameter data for spill fires

	Average Burning Rate (g/s)		Average Burning Duration (s)		Equivalent Initial Diameter (m)	
Volume (ml)	Gasoline	Denatured Alcohol	Gasoline	Denatured Alcohol	Gasoline	Denatured Alcohol
0.2	0.007	0.012	20	13	0.03	0.04
6.6	0.129	0.229	38	23	0.14	0.15
25	0.391	0.624	47	32	0.25	0.26
80	0.968	1.336	61	53	0.41	0.41
125	1.291	2.100	71	53	0.43	0.45
200	1.799	2.201	82	72	0.56	0.57
240	2.330	2.076	75	91	0.53	0.58
290	2.601	2.837	82	83	0.62	0.65
350	3.491	3.413	74	81	0.71	0.71
450	4.620	4.135	72	87	0.81	0.77

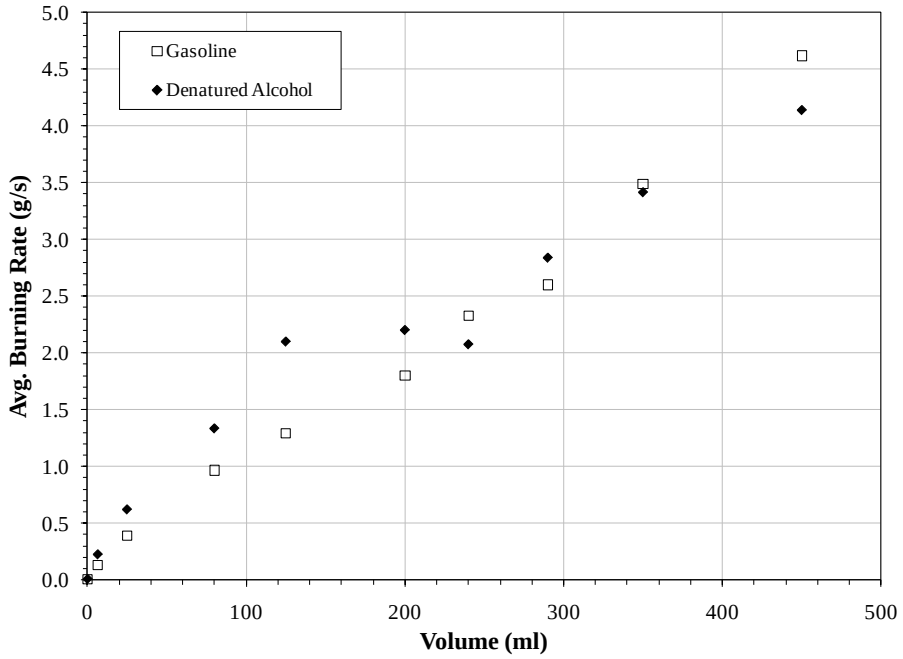

Figure 4-8 - Average burning rate vs. volume data for spill fires

Overall, the burning duration and burning rate values for denatured alcohol and gasoline were very close. This was not an expected outcome as gasoline generally has a significantly larger burning rate. However, this is quite possibly an artifact of the time averaging used to calculate the data. In fact, it was observed from the test videos that the gasoline fires tended to have a short duration, larger peak flame length. While on the other hand, most denatured alcohol fires had shorter peak flame

lengths with a longer duration. As was expected, both the burning rate and burning durations increased with increasing volume. However it seems that the burning durations leveled off to between 75 and 85 seconds as the volume increased.

In order to have some method of comparing the experimental spill fires to pool fire data found in the literature, burning rates (g/s) as a function of diameter were calculated from pool fire correlations presented in equations (5) and (6) from the radiatively dominated regime [Zabetakis et al., 1961]:

$$\dot{m}_f = \left[\dot{m}''_{max}\left(1 - e^{-k\beta D}\right)\right]\frac{\pi D^2}{4} \tag{5}$$

and the stagnant layer theory presented in Appendix A:

$$\dot{m}_f = \frac{\pi q_o D^{7/4}}{4} \tag{6}$$

The values used in equations (5) and (6) are:

Table 4-4 - Burning Rate Properties

	Gasoline	Denatured Alcohol	Units
$\kappa\beta$	2.1	2.5	(m^{-1})
$\dot{m}''_{max}$	0.055	0.015	(kg/s-m^2)
q_o	16.7	28.4	(kg/s-$m^{7/4}$)

The sources from which these properties were obtained can be seen in the complete list of liquid properties in Table B-3.

Figure 4-9 and Figure 4-10 show the comparison of burning rate from confined pool fire correlations stated above with experimental data for gasoline and denatured alcohol, respectively. It can be see that the experimental burning rate data for gasoline is between 20 and 30% of the corresponding calculated pool fire burning rate. While for denatured alcohol, the experimental burning rate is approximately

equal to the corresponding calculated pool fire burning rate. This difference in behavior is unusual, but can most likely be described by the fact that, as was noted before, the gasoline fires had peaks that seemed to have a short duration, while denatured alcohol spill fires had longer more steady peaks. This would mean that the average burning rate value for denatured alcohol is comparable to a steady state value, while that of gasoline is not due to its more transient nature.

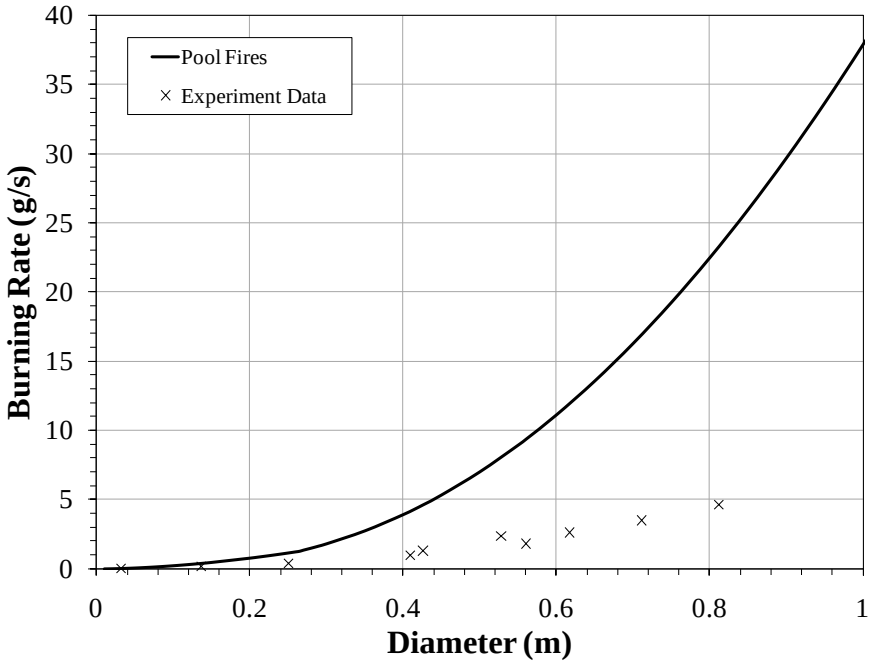

Figure 4-9 - Burning rate data for pool fires and experimental data for gasoline as a function of initial diameter

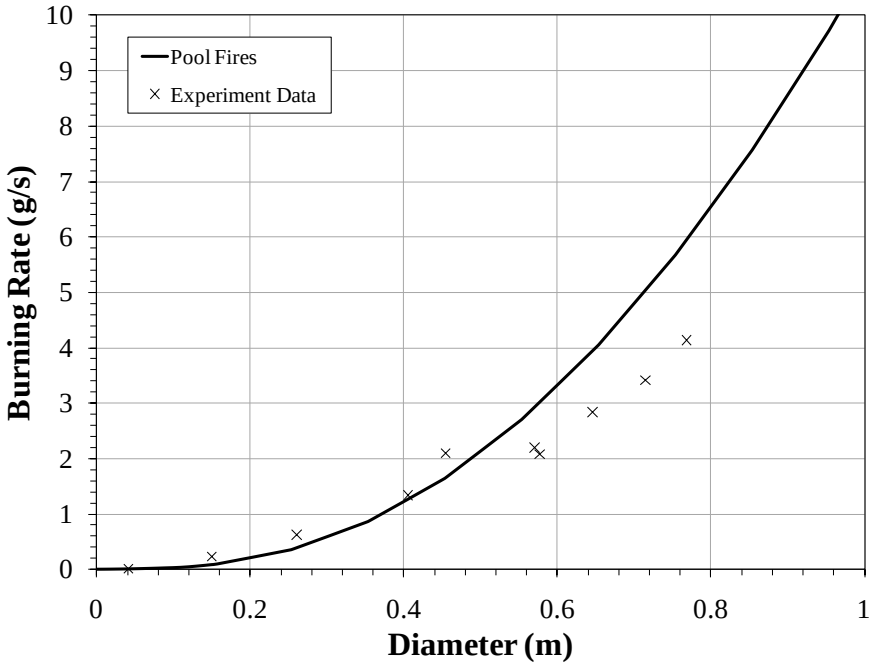

Figure 4-10 - Burning rate data for pool fires experimental data for denatured alcohol as a function of initial diameter

In order to explore the transient nature of the spill fire experiments, some sample flame diameter histories are shown in Figure 4-11 for two denatured alcohol and two gasoline spill fires. As a note, the sudden drop in the diameter in Figure 4-11d is due to a split of the pool into two (such as seen in Figure 4-4) pools during the test, the smaller of which extinguished in the time period consistent with the drop in diameter. The diameter of the 450 ml gasoline spill fire, in Figure 4-11a, has a very different profile than the other three diameter graphs in this figure. It seems to decrease in a much more rapid fashion, while the others stay fairly constant throughout the test. For all four tests presented, the flame lengths, however, decrease at a quicker rate than the diameter. One interesting thing to note is that after the first time step (5 seconds), the diameters of most of the fires grew slightly. It is unclear whether this growth is due to spreading that is still occurring at the time of ignition,

spread due to ignition, or simply flame spread across the fuel spill area. In addition, these increases tended to be small: on the order of 1 cm for the largest volumes. In relation to the diameter of the spill fires, this increase is very small.

The flame length and diameter histories seen in Figure 4-11 are fairly representative of most of the tests conducted in this research. It is for this reason that graphs for all forty tests are not shown. Something to reiterate is that it was observed that the gasoline pool fires tended to have a quicker and more intense peak flame height than the denatured alcohol spill fires which did not seem to have such a distinctly large peak at one point in the test. This can be seen when comparing the flame length histories of Figure 4-11a,b to Figure 4-11c,d.

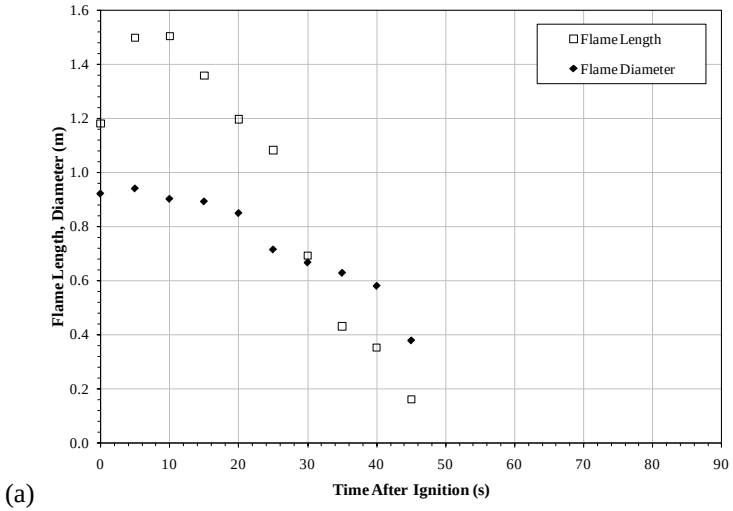

(a)

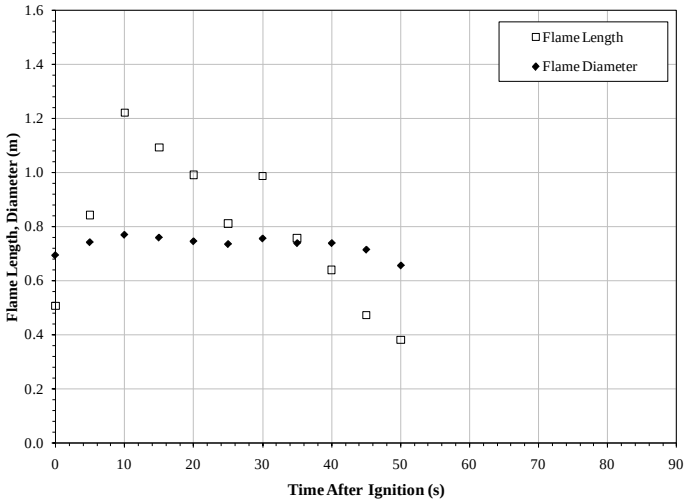

(b)

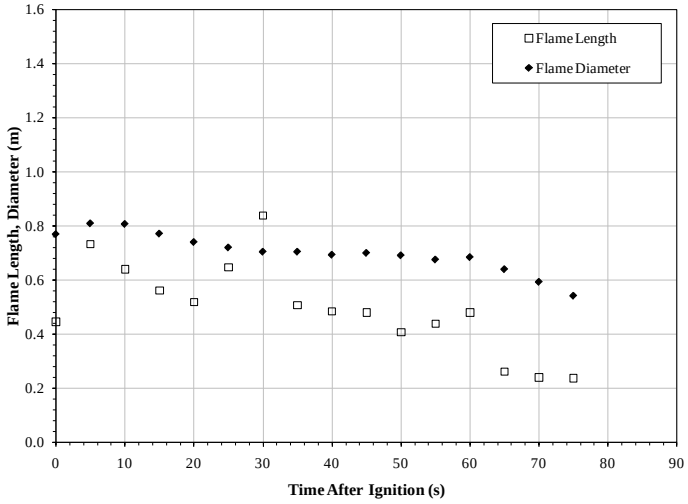

(c)

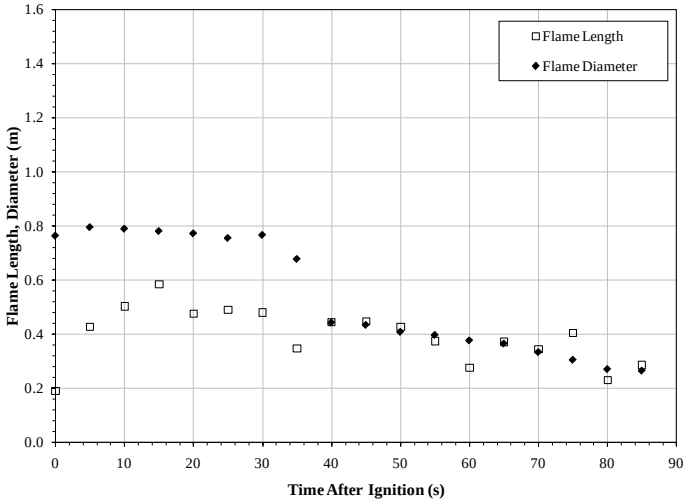

(d)

Figure 4-11 - Flame length and diameter test histories for: (a)450 ml gasoline, (b)240 ml gasoline, (c)450 ml denatured alcohol, and (d)240 ml denatured alcohol spill fire tests

5 A Liquid Spill Model

Liquid spread on a perfectly flat and impermeable surface can be described by various models and equations presented previously. In order to model a liquid spill, one must choose between determining the spill thickness via a transient or equilibrium method. For this research, the method choice is based somewhat on the method of the experiments conducted. The procedure of the spill fire tests called for the spill to stop spreading before igniting the fuel. This was done in order to be able to determine the initial burning area of the liquid spill. If a liquid spill was ignited before it stopped spreading, the initial spill area would be much more difficult to determine. In addition, coupling a transient spill thickness model with a burning rate model would entail too many complexities. Therefore, the spill model derived was one that considers a liquid spill at equilibrium.

The equations presented in Bradley [2002], Simmons et al. [2004] and Vignes-Adler [2002] are examples of the equilibrium spill height approach. These derivations use different forms of a balance of pressure and surface tension forces to determine an equilibrium spill depth. This type of approach also takes into account the interfacial interactions between the liquid and solid, which are not present in most transient models. In addition, while understanding the mechanics behind liquid spread is very important, for this study the end result (equilibrium spill height) is key. This parameter can be determined from one equation using a combination of liquid and liquid-surface properties.

The method used is similar to that of Vignes-Adler [2002]. The derivation is as follows. In order to proceed with this derivation, some assumptions must be made

about the surface interaction, which will be explored in later sections. The surface is assumed to be impermeable, perfectly flat, and perfectly level.

First, it must be recognized that a liquid spill on an impermeable surface is similar in behavior to a large drop as discussed in Section 1. This means that the edge of the liquid spill is similar to a sessile drop as seen in Figure 2-1, but has a flattened center as in Figure 5-1. Figure 5-1 shows the interfacial tensions and pressure forces acting on a large drop.

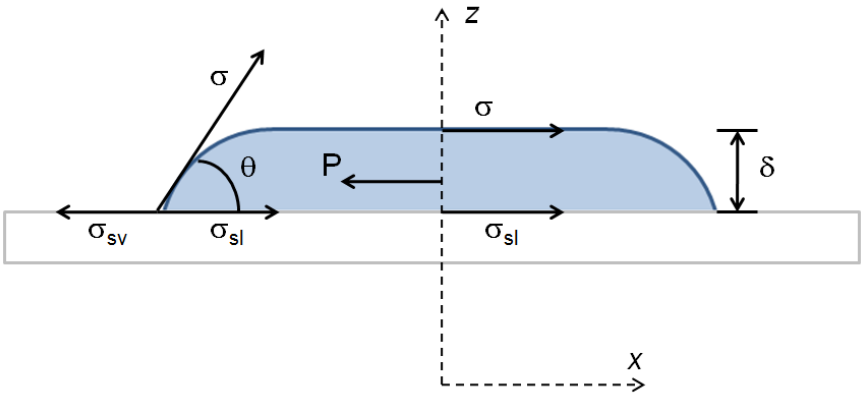

Figure 5-1 - Equilibrium shape of a large drop, with internal forces shown

Because the interfacial forces are directly proportional to their respective interfacial tensions, the equilibrium for the left side of the large drop in Figure 5-1 can be represented by the balance of interfacial tensions and the pressure forces:

$$\sigma_{sv} + P - \sigma - \sigma_{sl} = 0 \tag{7}$$

where P is the gravitational potential energy and p(z) is the hydrostatic pressure:

$$P = \int_0^{\delta} p(z)dz = \int_0^{\delta} \rho g z \, dz = \frac{1}{2}\rho g \delta^2 \tag{8}$$

And substituting (8) into (7), equation (7) becomes

$$\sigma_{sv} + \frac{1}{2}\rho g \delta^2 = \sigma + \sigma_{sl} \tag{9}$$

Recalling Young's equation as:

$$\cos(\theta) = (\sigma_{sv} - \sigma_{sl})/\sigma \tag{10}$$

We can combine Young's equation with equation (9), yielding:

$$\cos(\theta) = 1 - \frac{1}{2}\rho g \delta^2/\sigma \tag{11}$$

When equation (11) is solved for δ, one gets the equilibrium spill thickness equation:

$$\delta = \sqrt{\frac{2\sigma}{\rho g}(1 - \cos(\theta))} \tag{12}$$

One can see that in this equation, the equilibrium spill thickness is only dependent on the liquid and liquid-surface properties and not the spill configuration. This derivation produces results that are the same as the classical work of Batchelor [1967].

5.1 Model Comparison

The liquid spill thickness model, equation (12), was used to determine the theoretical spill thicknesses for the liquids used in the spill testing and spill fire testing. This was done using the liquid properties in Table 3-1, repeated below. These are compared to the average spill thicknesses and asymptotic spill thicknesses obtained from liquid and fuel spill testing (all volumes) in Table 5-1.

Table 5-1 - Theoretical and experimental spill thicknesses, with liquid properties

	Surface Tension (N/m)	Density[a] (kg/m^3)	Contact Angle (°)	δ, Theoretical (cm)	δ_{inf} (cm)	δ, Avg. Experimental (cm)
Water	0.072[b]	999.0	85[b]	0.366	0.250	0.221
3% AFFF	0.0172[c]	989.6	14.2[c]	0.033	0.069	0.054
6% AFFF	0.0172[d]	980.2	14.2[d]	0.033	0.061	0.051
Gasoline	0.0219[c]	790	19.7[c]	0.059	0.067	0.054
Denatured Alcohol	0.0223[c]	742	19.7[d]	0.058	0.069	0.054

a- Calculated
b- Average Literature Value
c- Experimentally Determined
d- Assumed equal to similar liquid

It can be seen that the theoretical spill thicknesses obtained agrees moderately well with both the average and asymptotic experimental values obtained. The best agreement is seen for the liquid fuels. However, the model tends to under-predict the experimental results for the 3% and 6% AFFF solutions and over-predicts the experimental result for water. The over-prediction for the water spill thickness is possibly due to the fact that there is a large range of possible contact angles found in the literature for water on concrete.

Some assumptions that this model makes include that the surface be impermeable and perfectly flat. These two assumptions are not present for the substrate used in testing. It was seen that in some areas of the concrete pad, there existed pooling, indicative of the surface not being perfectly flat. Also, the concrete used was not sealed, thus providing a somewhat permeable surface. While both of these surface characteristics were thought to have minimal impact for the substrate being used, it is possible that they could account for the differences observed between the experimental and theoretical results.

6 A Liquid Spill Fire Burning Rate Model

Current liquid spill fire models such as developed by Croce et al. [1986] and Cline et al. [1983] balance the burning rate of the liquid with a reduction in burning area, thus producing a diameter history as a function of time. However, these models use the steady-state burning rate obtained for pool fires (equation (2)) and do not account for any heat losses to the substrate. The intent of this spill model is to provide a method of determining spill fire burning rate that accounts for heat losses to the substrate.

Prior to beginning the derivation, some assumptions must be made. First, the spill thickness is assumed to be constant during burning. Evaporation prior to ignition is ignored and all liquid and substrate properties are assumed to be constant. In addition, this model would only work for fuels at or near their flashpoint temperature. For fuels below their flashpoint temperature, a more complicated heat transfer model would need to be employed in order to consider ignition. The validity of these assumptions will be addressed in a later section.

For a circular spill with constant thickness, the liquid mass, m_l is:

$$m_l = \rho_l \delta \frac{\pi}{4} D^2 \tag{13}$$

where, ρ_l is the liquid density, δ is the spill thickness determined with equation (12), and D is the spill diameter. The rate of change of the mass can be computed as the following:

$$\frac{dm_l}{dt} = \rho_l \delta \frac{\pi}{4} \frac{dD^2}{dt} \tag{14}$$

The mass loss from the liquid burning is:

$$\frac{dm_l}{dt} = -\dot{m}_f^{''} \left(\frac{\pi}{4} D^2\right) \tag{15}$$

where $\dot{m}_f^{''}$ is the burning rate of the liquid. Setting equation (14) equal to equation (15) and solving for the rate of change of D^2, we get a differential equation for the diameter of the spill as a function of the burning rate:

$$\frac{1}{D^2} \frac{dD^2}{dt} = \frac{-\dot{m}_f^{''}}{\rho_l \delta} \tag{16}$$

Since the spill fire diameter cannot be analytically determined on its own, an expression for the burning rate of the liquid must be found. This is accomplished through an energy balance for the liquid-substrate system. Figure 6-1 shows a schematic of the energy balance for the liquid and substrate during a fuel spill fire. The heat flux terms are defined as follows: $\dot{q}_{net}^{''}$ is the net heat flux from the flame and $q_k^{''}$ represents both the heat conduction through the liquid and the heat conduction into the solid substrate.

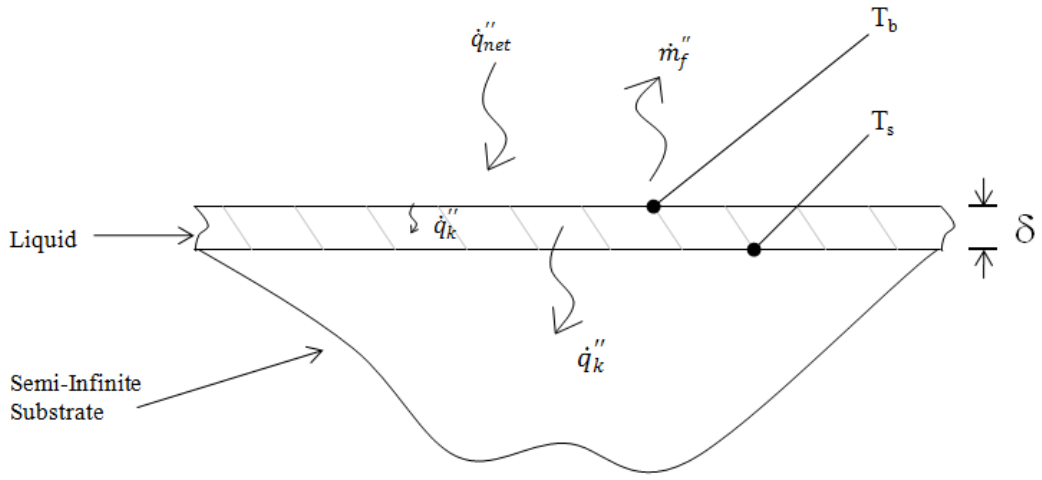

Figure 6-1 - Schematic of the energy balance for a fuel spill fire

Some assumptions were made when considering this energy balance. First, the liquid surface was assumed to be constant at the boiling temperature (T_b) and the substrate temperature was constant (T_s). An expression for the liquid and substrate energy balance is:

$$\dot{q}''_{net} - \dot{q}''_k = -\dot{m}''_f h_{fg} \tag{17}$$

where h_{fg} is the heat of vaporization for the fuel. The net heat flux from the flame can be found either by dividing the mass burning rate equation (49) from Appendix A, in the case of convectively dominated burning, or equation (2), in the case of radiatively dominant burning, by the latent heat of gasification (L), shown below. This assumes that the transient heat flux to the liquid spill behaves similarly to a steady state pool fire of the same instantaneous spill diameter.

$$\dot{q}''_{net} \cong \frac{q_o}{L} D^{-1/4} \tag{18}$$

$$\dot{q}''_{net} = \dot{q}''_{max} (1 - e^{-k\beta D}) \tag{19}$$

With $\dot{q}''_{max}$ being $\dot{m}''_{max}$ divided by the latent heat of gasification of the fuel, L. The latent heat of gasification can be defined as $L = h_{fg} + c_{p,l}(T_b - T_\infty)$. The boundary

between convectively dominated burning and radiatively dominated burning occurs at diameters of approximately 0.2m for most fuels [Babrauskas, 1983]. However, a different transition diameter will be used for this model. This diameter occurs at the intersection of the two equations. An explanation for this can be found in Appendix A.

Some care must be taken when representing the conduction heat losses into the substrate and the liquid as these are thought to have a significant impact burning rate of a liquid spill. First, since the liquid (T_b) and solid (T_s) surface temperatures were assumed to be constant, the conduction losses through the liquid are assumed to be quasi-steady:

$$\dot{q}''_{k,liquid} = \frac{k_l}{\delta}(T_b - T_s) \tag{20}$$

A solution for the transient heat flux at the surface of a solid with constant surface temperature (T_s) and initial temperature (T_∞) results in a transient thermal penetration depth, δ_{th}:

$$\delta_{th} = \sqrt{\pi \frac{k_s}{\rho_s c_{p,s}} t} \tag{21}$$

Treating the liquid-solid system as a composite material with liquid and solid thermal resistances of:

$$R_l = \frac{\delta}{k_l} \tag{22}$$

$$R_s = \frac{\delta_{th}}{k_s} = \sqrt{\frac{\pi t}{\rho_s k_s c_{p,s}}} \tag{23}$$

we can find the approximate transient conduction heat loss through the liquid and solid as:

$$\dot{q}_k^{''} = \frac{(T_b - T_\infty)}{R_l + R_s} = \frac{(T_b - T_\infty)}{\frac{\delta}{k_l} + \sqrt{\frac{\pi t}{\rho_s k_s c_{p,s}}}} \tag{24}$$

Now all of the key parts to this problem have been defined. Substituting equation (24) into equation (17), solving for $\dot{m}_f^{''}$ and substituting this result into (16), we get the final differential equation for D^2:

$$\frac{1}{D^2}\frac{dD^2}{dt} = \frac{-\dot{q}_{net}^{''} + \frac{(T_b - T_\infty)}{\frac{\delta}{k_l} + \sqrt{\frac{\pi t}{\rho_s k_s c_{p,s}}}}}{h_{fg}\rho_l \delta} \tag{25}$$

At this point, the derivation can take one of two paths for $\dot{q}_{net}^{''}$ depending on the initial diameter of spill. For an initial spill size in the convective regime, only the convective net heat flux needs to be used. For an initial spill size in the radiatively dominated regime, both the convectively and radiatively dominated regimes' net heat fluxes must be considered. A short explanation of this is that for an initially radiatively dominated spill, the $\dot{q}_{net}^{''}$ will be represented by equation (19) and the differential equation solved until the spill diameter enters the convectively dominated regime at which point $\dot{q}_{net}^{''}$ will be represented by equation (18). Solving the differential equation (16) is similar for both the convectively and radiatively dominated regimes. Only the derivation for the radiatively dominated regime will be shown, however the results for the convectively dominated regime will be stated later.

For the radiatively dominated regime, equation (16) becomes:

$$\frac{1}{D^2}\frac{dD^2}{dt} = \frac{-\dot{q}''_{max}\left(1-e^{-k\beta D}\right)+\dfrac{(T_b-T_\infty)}{\dfrac{\delta}{k_l}+\sqrt{\dfrac{\pi t}{\rho_s k_s c_{p,s}}}}}{h_{fg}\rho_l\delta} \tag{26}$$

At this time, it is prudent to non-dimensionalize this equation using the following dimensionless diameter, $\mathfrak{D}$, and time, τ:

$$\mathfrak{D} = \frac{D}{D_i} \tag{27}$$

$$\tau = \frac{t}{t_e} \tag{28}$$

where D_i is the initial spill diameter and t_e is the characteristic evaporation time scale defined as:

$$t_e = \frac{h_{fg}\rho_l\delta}{\dot{q}''_{max}} \tag{29}$$

The initial spill diameter, $D_{i,}$ can be calculated for a circular disc with a spill thickness δ from the volume of liquid, V, spilled using the following equation:

$$D_i = \sqrt{\frac{4V}{\pi\delta}} \tag{30}$$

Some additional constants must be defined in order to reduce the differential equation to its final form. The following characteristic conduction time t_k is defined as:

$$t_k = \frac{\delta^2}{k_l^2}(k\rho c_p)_s \tag{31}$$

The following characteristic time ratio, λ is introduced for convenience:

$$\lambda = \frac{t_e}{t_k} \tag{32}$$

And introducing a dimensionless constant, γ, defined as:

$$\gamma = \frac{(T_b - T_\infty)k_l}{\delta\ \dot{q}''_{max}} \tag{33}$$

will reduce equation (26) to the following:

$$\frac{1}{\mathfrak{D}^2}\frac{d\mathfrak{D}^2}{d\tau} = -\left(1 - e^{-k\beta\, D_i \mathfrak{D}}\right) + \frac{\gamma}{1 + \sqrt{\pi\tau\lambda}} \tag{34}$$

The resulting differential equation cannot easily be solved in closed form. Therefore an approximate method is used to find a solution. First, equation (34) should be integrated follows:

$$\int_1^{\mathfrak{D}^2} \frac{1}{\mathfrak{D}^2}\, d\mathfrak{D}^2 = \int_0^{\tau} \left(-\left(1 - e^{-k\beta\, D_i \mathfrak{D}}\right) + \frac{\gamma}{1 + \sqrt{\pi\tau\lambda}} \right) d\tau \tag{35}$$

$$\ln(\mathfrak{D}^2) = -\int_0^{\tau} \left(1 - e^{-k\beta\, D_i \mathfrak{D}}\right) d\tau + \frac{2\gamma}{\psi}\left(\sqrt{\tau} - \frac{\ln\left(1 + \psi\sqrt{\tau}\right)}{\psi}\right) \tag{36}$$

Where ψ is defined as:

$$\psi = \sqrt{\pi\lambda} \tag{37}$$

The remaining integral in equation (36) must be solved with the discrete approximation:

$$\int_0^{\tau} \left(1 - e^{-k\beta\, D_i \mathfrak{D}}\right) d\tau \cong \sum_{j=0}^{n} \left(1 - e^{-k\beta\, D_i \mathfrak{D}_j}\right) \Delta\tau \tag{38}$$

with:

$$\tau = n(\Delta\tau) \tag{39}$$

for a sufficiently small dimensionless time step, $\Delta\tau$. $\mathfrak{D}_j$ is the dimensionless diameter at time $\tau = j(\Delta\tau)$. Following a similar procedure for the convective burning case, the following is found:

$$\ln(\mathfrak{D}^2) = -\int_0^{\tau}\left(\frac{q_o}{\dot{q}''_{max}\,L}(D_i\mathfrak{D})^{-1/4}\right)d\tau + \frac{2\gamma}{\psi}\left(\sqrt{\tau} - \frac{\ln\left(1+\psi\sqrt{\tau}\right)}{\psi}\right) \tag{40}$$

and

$$\int_0^{\tau}\left(\frac{q_o}{\dot{q}''_{max}\,L}(D_i\mathfrak{D})^{-1/4}\right)d\tau \cong \sum_{j=0}^{n}\left(\frac{q_o}{\dot{q}''_{max}\,L}(D_i\mathfrak{D}_j)^{-1/4}\right)\Delta\tau \tag{41}$$

This model must be solved numerically, with a small time step. Using equations (40) and (36) one could find the mass burning rate as a function of time from the rate of change of the dimensionless diameter, using equation (16). This solution shows that the dimensionless diameter is a function of a variety of variables:

$$\mathfrak{D} = f\left(\tau, k\beta D_i, \gamma\,, \lambda = \frac{t_e}{t_k}\right) \tag{42}$$

These variables are dependent on time, the initial spill area, the fluid properties, as well as the substrate properties.

6.1 Model Comparison

Experiments conducted in this research were used to validate the spill fire model derived in Section 6 using air, liquid, and concrete properties presented in Table B-1 through Table B-3. The resulting model predictions are shown in Figure 6-2 with the corresponding dimensionless experimental data. Table 6-1 shows the dimensionless groups and characteristic variables used in this model for both fuels.

Table 6-1 - Dimensionless groups and characteristic variables from burning rate model for gasoline and denatured alcohol

	Gasoline	Denatured Alcohol	Units
ψ	1.35	0.53	N/A
t_e	23.84	6.83	(s)
λ	0.58	0.09	N/A
t_k	40.87	76.18	(s)
γ	0.91	0.21	N/A

The laminar burning rate was not included in the evaluation of this model because the experimental diameter results used did not enter this regime for the tests that were modeled. If one examines the parameters in Table 6-1, it can be inferred from the values of λ that the gasoline will burn at a faster rate than the denatured alcohol. λ is a ratio of the characteristic evaporation time and characteristic conduction time. A large characteristic conduction time means that conduction into the substrate is slow, while a low evaporation time means that the burning or evaporation would tend to be quicker.

Overall, the predictions made by the model were not very accurate. The model seems to capture the trends seen for the 450 ml and 240 ml denatured alcohol tests as seen in Figure 6-2c,d. And if it were not for the sudden drop in diameter for the 240 ml denatured alcohol test, which was due to splitting of the pool and extinguishment of the smaller pool, the model prediction would be very accurate for this test. The model does not predict the gasoline spill fires very well. The reason that the model does not predict the experimental results very well is most likely due to the fact that the experimental results were not obtained in a fashion that accurately determined the burning area of the liquid spill. This is not to say that the measurements are wrong but

that their interpretation is skewed. The experimental spill shapes were far from ideal in most cases: often having oblong shapes and various protrusions. Thus the seemingly random nature of spill shape would make it difficult to experimentally determine a spill diameter that would accurately characterize the burning rate. In retrospect, it would have been better practice to have captured video along two or more axes in order to get an understanding of the shape of the spill fire as a function of time rather than in just one axis. Despite the doubts about the accuracy of this model, it should not be discounted based on the experimental methods used. Further validation should be undertaken using different experimental methods meant to capture an accurate spill area versus time or the mass burning rate versus time.

Further inspection of this model shows that in some cases, the initial heat loss to the substrate could be greater than the net heat flux from the flame, depending on spill size. This could be due to a variety of factors including assumptions made for liquid and substrate properties. This would cause the fire diameter to increase, which is an unrealistic result. In addition, extinguishment in the model does not seem to be very accurate. It can be seen from the Figure 6-2a,d that near extinguishment (i.e. the end of experimental data) there is still significant amounts of fuel left in the pool as shown by the model. And although at the end of most tests, there was some residual fuel on the substrate, the amounts were very small. This behavior is puzzling, however it could be an artifact of the means of describing extinguishment for the experimental data or from the fact that extinction is not modeled.

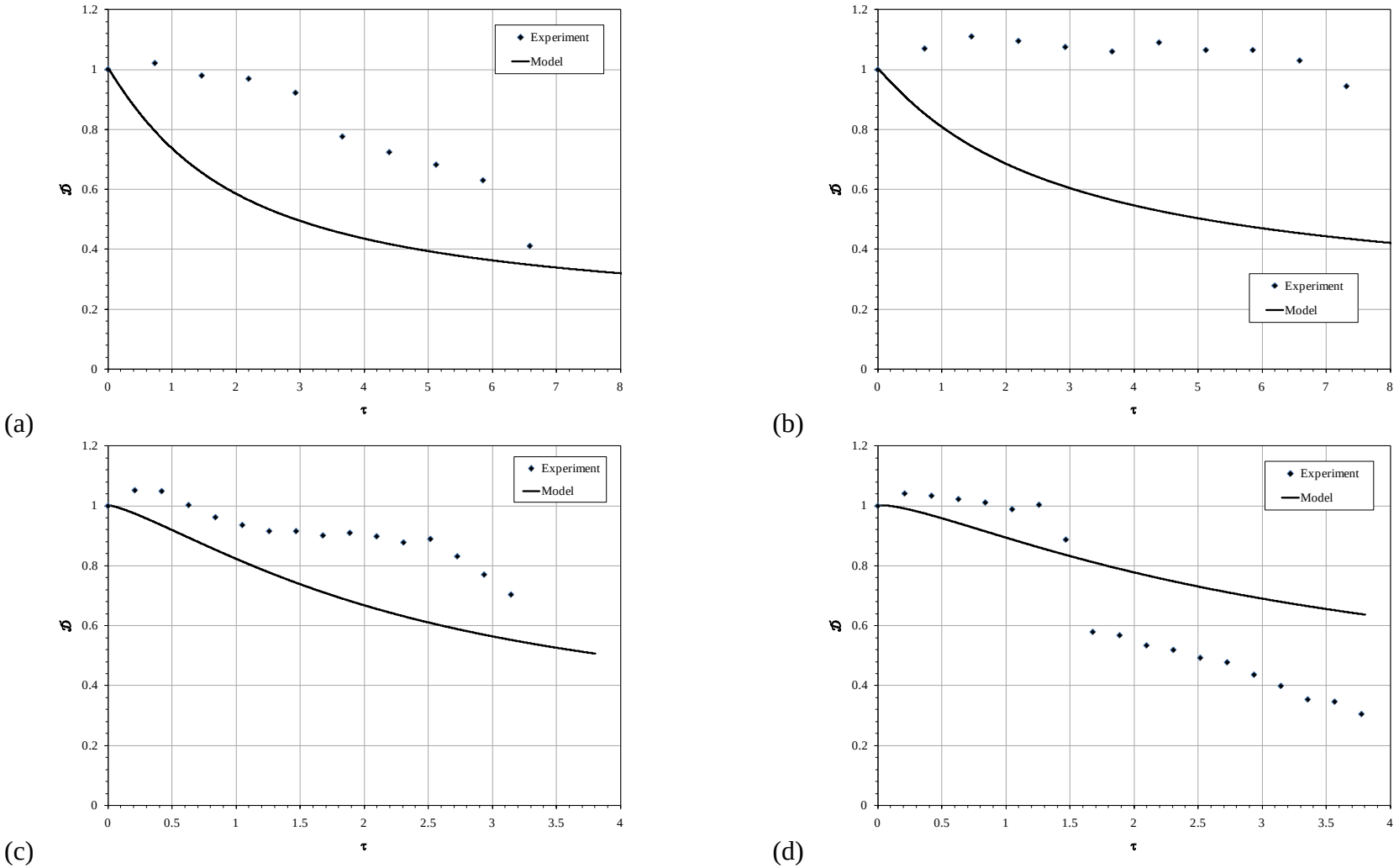

Figure 6-2 - Experimental results and model predictions for: (a)450 ml gasoline, (b)240 ml gasoline, (c)450 ml denatured alcohol, and (d)240 ml denatured alcohol spill fire tests

The spill fire model has varying results based on the spill fire scenario in question. Due to the inherent complexities of spill fires, there are a few possible reasons that the spill fire model does not accurately represent the spill fire experimental results, other than the difficulties with the experimental data as discussed beforehand. There were a few assumptions that were made while deriving the spill fire model, including: constant liquid properties, constant spill thickness, circular shape, and quasi-steady conduction through the liquid. For most fuels and fuel properties, the constant property assumption is valid, however Okamoto et al. [2009] showed that the boiling temperature of gasoline is not constant, but will increase as the more volatile components are evaporated and burned first.

The constant spill thickness assumption is one that also presents some interesting complexities. First of all, the experimental spill thickness obtained is an average over the spill area, where in some parts of the spill it could be thinner and some deeper. These differences are due to surface imperfections and would likely have a significant impact on the local burning rate of the spill in some areas. Temperature of a liquid has been shown to have an impact on surface tension. Temperature tends to decrease the surface tension of a liquid, this has been shown for methanol by Souckova et al. [2008] and for various fuels by [SFPE, 2002]. However, according to Young's law the contact angle would increase with increasing temperature, assuming $\sigma_{sl} - \sigma_{sg}$ is relatively constant. This would in turn negate the impact of decreasing surface tension on the theoretical spill thickness presented in equation (12). However, if the interfacial tensions σ_{sl} and σ_{sg} also decrease with temperature, the difference between the two would probably not change very much. Increases in temperature produce a

decrease in density for most liquid fuels, which would further cause the spill thickness found in equation (12) to increase. When examining the impact of these property changes on the spill height equation, there is a relatively small difference in the resulting spill thickness.

The maximum burning rate per unit area can be determined from the model with ($\gamma \neq 0$) and without ($\gamma = 0$) heat losses. The resulting burning rates are plotted as a function of initial spill diameter along with those found in the pool fire correlation for methanol in Figure 6-3. It can be seen that the model with heat loss does predict burning rates that are lower than those for steady-state pool fires. However, when not including heat loss in the model, the results become larger than those found from pool fire correlations. Similar results were found for gasoline. These results are promising because they show that the model does in fact produce a lower burning rate than the pool fire correlation, which is due to the heat loss term. Further exploration of these decreases will now be discussed.

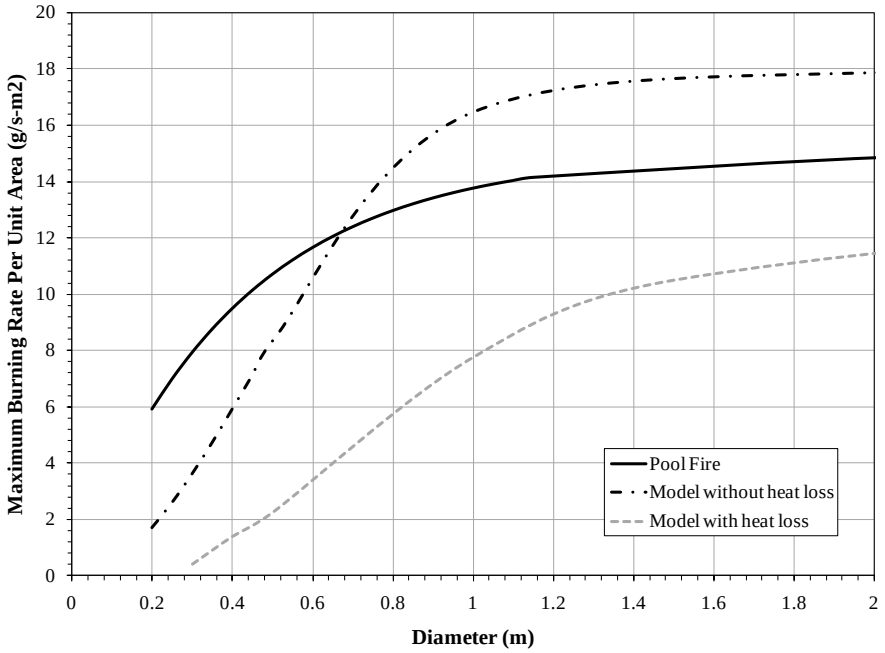

Figure 6-3 - Maximum burning rates per unit area for ethanol: from spill fire model and pool fire correlation (initial spill diameter used for the model results)

The spill fire burning rate model was used to calculate the average burning rates for some scenarios. When compared to finding the peak burning rates from the model, it was often difficult to calculate an average burning rate due to limitations in the numerical calculation method. These results are presented in Figure 6-4 and Figure 6-5 along with experimental data and data from pool fire correlations discussed previously. It can be seen for the gasoline case that the model average burning rate predictions tend to follow the same trend as the experimental data, being approximately 20-30% of the burning rate from pool fire correlations.

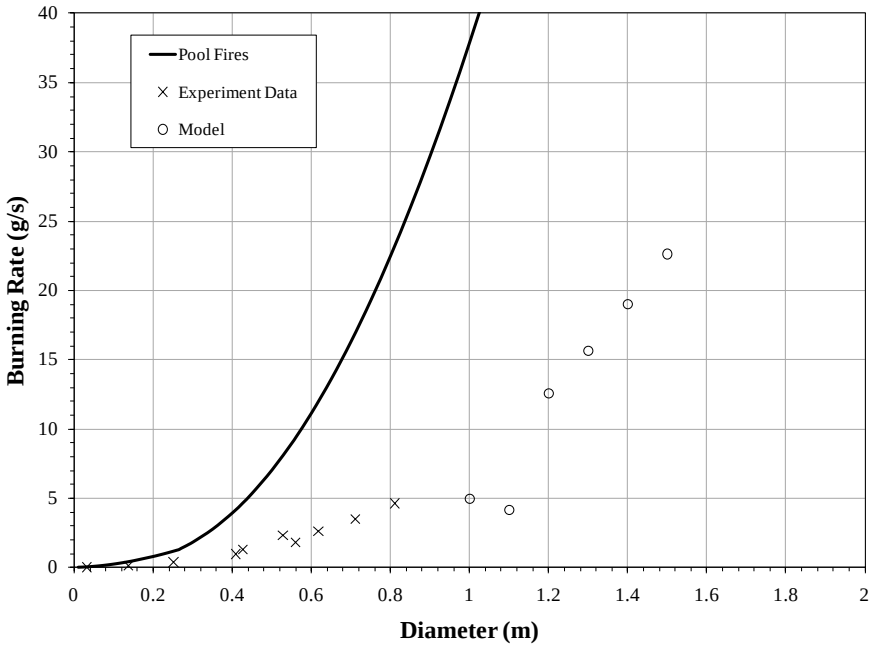

Figure 6-4 - Average burning rate predictions for gasoline from model with experimental data and pool fire correlation

On the other hand, the model results for denatured alcohol, Figure 6-5, did not follow the trend of the experimental results. However, the model did produce results that were the same order of magnitude as the experimental results and showed an increasing trend in burning rate for increasing initial diameter. Both the denatured alcohol and gasoline average burning rate predictions show a burning rate that is significantly less than the steady stat pool fire burning rates. This agrees with other experimental results found in the literature: [Putorti et al., 2001] and [Gottuk et al., 2001].

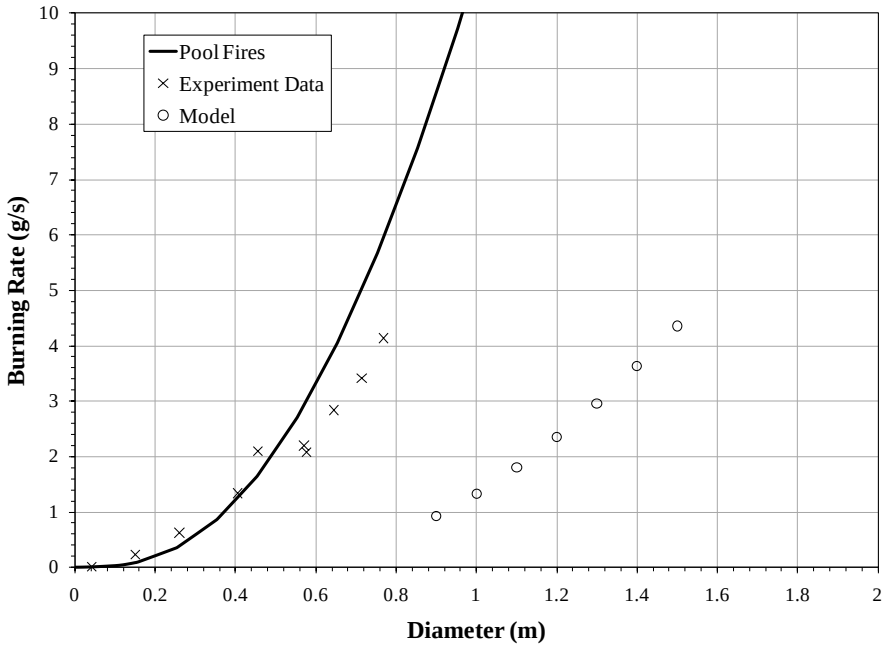

Figure 6-5 - Average burning rate predictions for denatured alcohol from model with experimental data and pool fire correlation

7 Conclusions

The aim of this research was to develop a method for predicting the spill dynamics and burning dynamics of a liquid fuel fire. Two models were developed in order to address the spill thickness and spill fire burning dynamics of liquid fuels. In addition, two liquids were spilled to provide an alternative, experimental method for determining a fuel spill thickness based on a liquid with similar properties. Subsequent sections will address the performance of these methods and outline possible means to improve these methods.

7.1 Liquid Spills

Overall, it seems that both the experimental and theoretical methods produced predictions of liquid fuel spill thicknesses that were very accurate. The following results were found for volumes of liquids ranging from 0.2 ml to 450 ml. The asymptotic spill thicknesses found experimentally were 0.25, 0.069, 0.061, 0.067, and 0.069 cm for water, 3%AFFF, 6%AFFF, gasoline, and denatured alcohol, respectively. The average spill thicknesses determined experimentally were: 0.221, 0.054, 0.051, 0.054, and 0.054 cm for water, 3%AFFF, 6%AFFF, gasoline, and denatured alcohol, respectively. And the theoretically determined spill thicknesses were: 0.0366, 0.033, 0.033, 0.059, and 0.058 cm for water, 3%AFFF, 6%AFFF, gasoline, and denatured alcohol, respectively. Therefore, two different methods exist that can, with varying levels of accuracy based on the liquid in question, be used to determine the spill thickness of a liquid fuel. And one could use one of the methods above to find the potential spill area from a given volume of liquid fuel in order to assess hazards. It was found that spill thicknesses for water, 3%AFFF, 6%AFFF, gasoline and denatured alcohol exhibit an exponential behavior with respect to volume spilled when spilled on the concrete substrate used. The properties that had the most impact on spill thickness were surface tension and contact angle. That being said, it is important to determine these for whatever liquid and substrate combination that is being evaluated.

For most fuels spilled on concrete, spill thicknesses should be on the order of 0.1 cm or less. If a fuel that has an unusually large surface tension, approaching that of water, the corresponding spill thickness should be greater than 0.1 cm. The

importance of substrate characterization, both through physical properties and topography has been found to be very important in determining the extent of a spill on that substrate. Surface permeability, surface flatness, and liquid-solid contact angle can all have a significant impact on the spill behavior of a liquid. When approximating the spill thickness of a liquid on an imperfect substrate, experimental methods rather than theoretical methods would be suggested.

7.2 Fuel Spill Fires

While the burning rate model does not seem to accurately predict the spill fire diameters found through experiments, some promising results such as those shown in Figure 6-3, Figure 6-4, and Figure 6-5, lend credit to the approach used because they show the decrease in burning rate produced by the spill fire model. Experimental spill fire results showed average burning rates that were approximately 20-30% of the corresponding pool fire burning rates for gasoline and closely approximated for denatured alcohol. Thus it seems that when approximating a spill fire, it is unclear whether or not pool fire correlations found in the literature are applicable. The spill fire model, which is still in development provides more qualitative than quantitative results at this point. More validation is required for the spill fire model using different methods than used in this research. The experimental conditions tested in this research, while not ideal; are practical spill fire scenarios and produce valuable data. In some cases, the initial burning rate predicted by the spill fire model was negative. This is a non-physical behavior, but suggests that the initial heat losses should be examined more closely.

8 Future Research

In order to properly evaluate the spill fire model presented in this work, it would be necessary to conduct experiments that more closely resembled an ideal configuration. This would include spilling the flammable liquids atop an impermeable substrate that is closer to being perfectly flat and level, compared to the concrete used in this study.

In addition, in order to accurately model the burning behavior of a more practical spill fire scenario such as those experiments conducted in this research, significant modifications must be made to the experimental setup, such as mass loss measurements for calculating burning rate measurements. Vital information about spill fire dynamics is lost when only average values (i.e. average burning rate) are able to be calculated. In order to have an accurate method for comparing burning rates from spill fires to pool fires, a more accurate measure of the peak burning rate and peak burning duration should be determined. This was not possible with the experimental methods used in this research.

At this point, not all of the video footage has been analyzed with respect to the flame diameters and flame lengths as a function of time for the entire set of spill fires. These should be further analyzed in order to obtain a full set of data that can be compared to model predictions. The subject of spill fire breakup into smaller pools should be further examined. This seemed to be a phenomenon that could arise due to a variety of conditions including pool geometry, surface topography, etc., however

the concept is not fully understood. Extinction of a spill fire should be examined as it relates to the physical phenomenon as well as impacts on the spill fire model.

Current research is being conducted under the same grant (NIJ Award No. 2008-DN-BX-K168) as this work to examine spill fires atop various residential and commercial substrates. The spill fire model developed in this research should be applied to other experimental data such as those found in the current research mentioned, in order to analyze its validity.

Appendix A - Convective Burning Rate Calculation

The burning rate of a liquid pool in the convective regime has not been characterized in a form such as seen for radiatively dominated burning in equation (2). Therefore, the convective burning rate must be calculated from the stagnant layer solution provided in Quintiere [2006]. This shows the fuel burning rate to be approximately equal to:

$$\dot{m}_f'' \cong \frac{h_c}{c_p}\ln(1+B) \tag{43}$$

were h_c is the convective heat transfer coefficient, c_p is the specific heat of the fuel, and B is the Spalding B number for the fuel. The B number represents the ratio of chemical energy released from combustion to the energy required to vaporize the fuel [Quintiere, 2006]. Both the B number and c_p are readily available from the literature for various fuels. The convective heat transfer coefficient is dependent on the pool configuration. This can be found from the Nusselt number (Nu) correlation for natural convection on a flat plate [Incropera, 2007]:

$$Nu = 0.54 Ra_D^{1/4} \tag{44}$$

for the laminar case with 10^4<Ra<10^7 and where

$$Nu = \frac{h_c D}{k} \tag{45}$$

by definition. k is the thermal conductivity of air and D is the diameter. Equation (44) is valid for diameters up to approximately 0.15m for the fuels used in this testing. This is important to note because the radiatively dominated regime begins at

diameters of approximately 0.2m. The treatment of this will be discussed at the end of this section. The Rayleigh number (Ra) is by definition:

$$Ra_D = \frac{g\beta}{\nu\alpha}(T_s - T_\infty)D^3 \tag{46}$$

where β is the expansion coefficient, ν is the kinematic viscosity for air, α is the thermal diffusivity for air, T_s is surface temperature, and T_∞ is the ambient temperature. β can be represented by:

$$\beta = \frac{2}{(T_s + T_\infty)} \tag{47}$$

Substituting equations (45), (46), and (47) into equation (44), and solving for h_c, one finds:

$$h_c = CD^{-1/4} \tag{48}$$

with C being some constant. Substituting this into equation (43), we find the mass burning rate for a liquid pool in the convective regime to be:

$$\dot{m}_f'' \cong q_o D^{-1/4} \tag{49}$$

where q_o is a convective burning rate constant with units of kg/s-$m^{7/4}$ equaling:

$$q_o = 0.54\frac{k}{c_p}\ln(1+B)\left(\frac{g\beta}{\nu\alpha}(T_s - T_\infty)\right)^{1/4} \tag{50}$$

Now the burning rate of a liquid pool in the convectively dominated regime can be characterized knowing some air properties, the fuel properties, and the size of the pool in question using equations (49) and (50). As mentioned previously, there is an issue with the boundary that separates the use of the radiatively dominated and convectively dominated burning equations.

Appendix B - Liquid and Substrate Properties Used in Spill Fire Model

Table B-1 - Air Properties

	Air	Units	Source
ν	20.92	$10^{-6}(m^2/s)$	[Incropera, 2007]
α	29.9	$10^{-6}(m^2/s)$	[Incropera, 2007]
k	30.0	10^{-3}(kW/m-K)	[Incropera, 2007]
T_∞	298	(K)	N/A
g	9.8	(m^2/s)	N/A

Table B-2 - Concrete Properties

	Concrete	Units	Source
k	0.0014	(kW/m-K)	[Incropera, 2007]
ρ	2224	(kg/m^3)	Section 3.1.1
c_p	0.88	(kJ/kg-K)	[Incropera, 2007]

Table B-3 - Gasoline and Denatured Alcohol Properties

				Source	
	Gasoline	Denatured Alcohol	Units	Gasoline	Denatured Alcohol
T_b	318	351	(K)	[Quintiere, 2006]	[Quintiere, 2006]
c_p	2.10	2.40	(kJ/kg-K)	Estimated	[Quintiere, 2006]
L	330	1000	(kJ/kg)	[Babrauskas, 1983]	[Babrauskas, 1983]
ρ	742	790	(kg/m^3)	Table 3-1	Table 3-1
k	0.11	0.14	10^{-3}(kW/m-K)	[HB of Aviation Fuels]	Estimated
h_{fg}	288	837	(kJ/kg)	Estimated	[SFPE, 2003]
δ	0.059	0.058	(cm)	Table 5-1	Table 5-1
$\kappa\beta$	2.1	2.5	(m^{-1})	[Babrauskas, 1983]	[Babrauskas, 1983]
$\dot{m}''_{max}$	0.055	0.015	$(kg/s\text{-}m^2)$	[Babrauskas, 1983]	[Babrauskas, 1983]
θ	19.7	19.7	$(^o)$	Table 3-1	Table 3-1
σ	0.0219	0.0223	(N/m)	Table 3-1	Table 3-1
B	9.1	3.1	N/A	Estimated	[Quintiere, 2006]

Appendix C - Liquid Spill and Spill Fire Data

Table C-1 - Spill data for water experiments

Liquid	Volume (ml)	Spill Area (cm^2)	Spill Depth (cm)	Spill Depth Difference from volume avg. (%)
Water	0.2	1.73	0.116	18.3
	0.2	2.72	0.074	-28.7
	6.65	43.5	0.153	0.5
	6.65	43.9	0.151	-0.5
	25	127	0.196	-9.3
	25	108	0.232	7.8
	80	338	0.237	-4.0
	80	313	0.256	3.7
	125	500	0.250	10.3
	125	629	0.199	-12.9
	200	792	0.253	0.5
	200	800	0.250	-0.6
	240	951	0.252	8.9
	240	1158	0.207	-10.8
	290	1015	0.286	6.4
	290	1164	0.249	-7.3
	350	1445	0.242	-0.1
	350	1441	0.243	0.1
	450	1772	0.254	-12.3
	450	1421	0.317	9.9

Table C-2 - Spill data for 3% AFFF experiments

Liquid	Volume (ml)	Spill Area (cm^2)	Spill Depth (cm)	Spill Depth Difference from volume avg. (%)
3% AFFF	0.2	11.3	0.018	0.7
	0.2	11.5	0.017	-0.7
	6.65	166	0.040	5.1
	6.65	185	0.036	-5.7
	25	604	0.041	2.7
	25	639	0.039	-2.9
	80	1614	0.050	0.8
	80	1639	0.049	-0.8
	125	2058	0.061	8.8
	125	2500	0.050	-10.7
	200	2384	0.084	10.7
	200	3029	0.066	-13.5
	240	4793	0.050	-49.9
	240	2400	0.100	25.0
	290	3707	0.078	3.5
	290	3987	0.073	-3.8
	350	3831	0.091	5.8
	350	4331	0.081	-6.5
	450	9300	0.048	-24.0
	450	6287	0.072	16.2

Table C-3 - Spill data for 6% AFFF experiments

Liquid	Volume (ml)	Spill Area (cm^2)	Spill Depth (cm)	Spill Depth Difference from volume avg. (%)
6% AFFF	0.2	10.9	0.018	-21.7
	0.2	7.58	0.026	15.2
	6.65	175	0.038	-1.8
	6.65	169	0.039	1.7
	25	492	0.051	10.8
	25	628	0.040	-13.8
	80	1554	0.051	5.1
	80	1730	0.046	-5.7
	125	1995	0.063	-7.0
	125	1752	0.071	6.1
	200	3321	0.060	0.4
	200	3349	0.060	-0.4
	240	4125	0.058	-5.4
	240	3724	0.064	4.9
	290	6164	0.047	-3.2
	290	5798	0.050	3.0
	350	4510	0.078	11.4
	350	5841	0.060	-14.8
	450	6069	0.074	N/A

Table C-4 - Spill fire data for gasoline experiments

Liquid	Volume (mL)	Weight (g)	Spill Area (cm^2)	Spill Depth (cm)	Spill Depth Difference from volume avg. (%)	Equivalent Initial Diameter (m)	Burning Duration (s)	Burning Duration Difference from volume avg. (%)	Average Burning Rate (g/s)	Avg. Burning Rate Difference from volume avg. (%)
Gasoline	0.2	NM	11.9	0.012	-78.8	0.04	19	-2.6	0.008	2.5
	0.2	NM	4.6	0.032	30.6	0.02	20	2.5	0.007	-2.6
	6.6	4.7	158	0.030	-10.5	0.14	40	6.3	0.12	-9.6
	6.6	4.9	136	0.036	8.7	0.13	35	-7.1	0.14	8.0
	25	18	458	0.040	7.4	0.24	52	9.6	0.35	-11.2
	25	18	532	0.034	-8.7	0.26	42	-11.9	0.43	9.2
	80	59	1270	0.046	3.1	0.40	57	-7.0	1.03	5.9
	80	59	1363	0.043	-3.3	0.42	65	6.2	0.91	-6.6
	125	91	1311	0.069	7.7	0.41	72	2.1	1.27	-2.0
	125	91	1544	0.059	-9.1	0.44	69	-2.2	1.32	1.9
	200	145	2516	0.058	-2.7	0.57	77	-5.8	1.89	4.6
	200	147	2420	0.061	2.6	0.56	86	5.2	1.71	-5.1
	240	175	2294	0.076	-5.0	0.54	77	2.6	2.27	-2.8
	240	175	2089	0.084	4.5	0.52	73	-2.7	2.39	2.7
	290	212	3183	0.066	-6.6	0.64	75	-9.3	2.82	7.8
	290	212	2814	0.075	5.8	0.60	89	7.9	2.38	-9.3
	350	258	4365	0.059	-10.2	0.75	70	-5.7	3.69	5.4
	350	257	3604	0.071	8.5	0.68	78	5.1	3.29	-6.1
	450	331	5566	0.059	-7.5	0.84	69	-3.6	4.80	3.7
	450	329	4801	0.068	6.5	0.78	74	3.4	4.44	-4.0

NM - Not Measured

Table C-5 - Spill fire data from denatured alcohol experiments

Liquid	Volume (mL)	Weight (g)	Spill Area (cm^2)	Spill Depth (cm)	Spill Depth Difference from volume avg. (%)	Equivalent Initial Diameter (m)	Burning Duration (s)	Burning Duration Difference from volume avg. (%)	Average Burning Rate (g/s)	Avg. Burning Rate Difference from volume avg. (%)
Denatured Alcohol	0.2	NM	16.8	0.010	-29.0	0.05	12	-8.3	0.013	7.1
	0.2	NM	10.6	0.015	18.4	0.04	14	7.1	0.011	-8.3
	6.6	5.5	188	0.029	-2.1	0.15	25	8.0	0.22	-4.1
	6.6	5.0	165	0.030	2.0	0.14	21	-9.5	0.24	3.8
	25	20	477	0.042	10.0	0.25	34	5.9	0.59	-6.1
	25	20	591	0.034	-12.5	0.27	30	-6.7	0.66	5.4
	80	72	1426	0.050	-8.2	0.43	51	-2.9	1.41	5.2
	80	68	1163	0.059	7.0	0.38	54	2.8	1.26	-5.8
	125	99	1462	0.068	9.8	0.43	70	25.0	1.41	-48.8
	125	98	1795	0.054	-12.1	0.48	35	-50.0	2.79	24.7
	200	152	2411	0.063	4.2	0.55	81	11.7	1.88	-17.0
	200	156	2699	0.058	-4.6	0.59	62	-15.3	2.52	12.7
	240	187	2651	0.070	-1.9	0.58	87	-4.0	2.15	3.4
	240	188	2574	0.073	1.8	0.57	94	3.7	2.00	-3.6
	290	230	2837	0.081	12.3	0.60	97	14.4	2.37	-19.9
	290	228	3740	0.061	-16.3	0.69	69	-20.3	3.31	14.2
	350	276	4114	0.067	-2.6	0.72	85	4.7	3.25	-5.1
	350	276	3909	0.071	2.4	0.71	77	-5.2	3.58	4.7
	450	356	4590	0.078	1.2	0.76	79	-9.5	4.51	8.2
	450	354	4674	0.076	-1.2	0.77	94	8.0	3.76	-9.9

NM - Not Measured

References

Babrauskas, Vytenis. "Estimating Large Pool Fire Burning Rates." *Fire Technology* 19 (1983): 251-61.

Batchelor, G. K. *An Introduction to Fluid Dynamics*. Cambridge: U.P., 1967.

Belore, R.C., and I.A. Buist. *Modelling of Oil Spills in Snow*. Rep. Ottawa, Canada: S.L. Ross Environmental Research Limited, 1988.

Blinov, V., and G. Khudyakov. *Diffusion Burning of Liquids*. Rep. US Army Translation, 1961. NTIS No. AD296762.

Bradley, D., *Model for Pool Fires Following Chemical Agent Spills*. Rep. Abingdon, MD: Science Applications International Corporation, 2002.

Chambers, G. *Flight Line Extinguisher Evaluation*. Rep. no. DOD-AGFSRS-76-9. US Air Force, 1977.

Cline, D., and L. Koenig. "The Transient Growth of an Unconfined Pool Fire." *Fire Technology* (1983): 149-62.

Croce, P., and K. Mudan. "Calculating Impacts for Large Open Hydrocarbon Fires." *Fire Safety Journal* 11 (1986): 99-112.

DeHaan, J. D. "The Influence of Temperature, Pool Size, and Substrate on the Evaporation Rates of Flammable Liquids." *Interflam* (1999): 1179-187.

Garo, J., H. Koseki, J. Vantelon, and C. Fernandez-Pello. "Combustion of Liquid Fuels Floating on Water." *Thermal Science* 11.2 (2007): 119-40.

Gottuk, D., J. Scheffey, F. Williams, J. Gott, and R. Tabet. *Optical Fire Detection for Military Aircraft Hangars: Final Report on OFD Performance to Fuel Spill Fires and Optical Stresses*. Rep. no. NRL/MR/6180—00-8457. Naval Research Laboratory, 2001.

Grimaz, S., S. Allen, J. Stewart, and G. Dolcetti. "Predictive Evaluation of Surface Spreading Extent for the Case of Accidental Spillage of Oil on the Ground." *ICheaP-8.* Vol. 11. Naples: Italian Association of Chemical Engineering AIDIC, 2007. 389-94.

Hayasaka, H. "Unsteady Burning Rates of Small Pool Fires." *5th Symposium on Fire Safety Science* (1997): 499-510.

Hill, S., J. Scheffey, F. Walker, and F. Williams. *Tests of Alternative Fire Protection Methods for USAF Hangars*. Rep. no. 8337. Naval Research Laboratory Memorandum, 1999.

Hottel, H. "Review -- Certain Laws Governing Diffusive Burning of Liquids, by V. I. Blinov and G. N. Khudyakov." *Fire Research Abstracts and Reviews* 1 (1958): 41-44.

Incropera, Frank P., David P. Dewitt, Theodore L. Bergman, and Adrienne S. Lavine. *Fundamentals of Heat and Mass Transfer.* Hoboken, NJ: John Wiley, 2007.

Iqbal, N., and M.H. Salley. *Fire Dynamics Tools Quantitative Fire Hazard Analysis Methods for the U.S. Nuclear Regulatory Commission Fire Protection Inspection Program*. NUREG-1805. Washington D.C.: U.S. Nuclear Regulatory Commission, 2004.

"Liquid Fuel Fires." *SFPE Handbook of Fire Protection Engineering*. 3rd ed. Quincy, Mass.: National Fire Protection Association, 2002. Print.

Keller, J. M., and C. S. Simmons. *The Influence of Selected Liquid and Soil Properties on the Propagation of Spills Over Flat Permeable Surfaces*. Rep. Pacific Northwest National Laboratory, 2005.

Kligys, M., A. Laukatis, M. Sinicas, and G. Sezemana. "The Influence of Some Surfactants on Porous Concrete Properties." *Materials Science* 14.4 (2007): 310-16.

"Liquid Fuel Fires." *SFPE Handbook of Fire Protection Engineering*. 3rd ed. Quincy, Mass.: National Fire Protection Association, 2002.

Modak, A.T. *Ignitability of High-Fire-Point Liquid Spills*. Rep. no. EPRI NP-1731. Norwood, MA: Factory Mutual Research, 1981.

Okamoto, K., N. Watanabe, Y. Hagimoto, K. Miwa, and H. Ohtani. "Changes in Evaporation Rate and Vapor Pressure of Gasoline with Progress Evaporation." *Fire Safety Journal* 44 (2009): 756-63.

Putorti, A.D., J.A. McElroy, and D. Madrzykowski. *Flammable and Combustible Liquid Spill/Burn Patterns*. Rep. no. 604-00. Washington D.C.: National Institute of Justice, 2001.

Quintiere, James G. *Fundamentals of Fire Phenomena*. Chichester, UK: Wiley, 2006. Print.

Raj, Phani P. K., and Ashok S. Kalelkar. *Assessment Models in Support of the Hazard Assessment Handbook*. Rep. no. CG-D-65-74. Department of Transportation, 1974.

Rousseau, Jacques. *Water Flow by Means of Capillary Action*. Tech. Air-Ins Inc, 1993. Web. 14 Apr. 2010.

Simmons, C. S., J. M. Keller, and J. L. Hylden. *Spills on Flat Inclined Pavements*. Rep. no. PNNL-14577. Richland, Washington: Pacific Northwest National Laboratory, 2004.

Souckova, M., J. Klomfar, and J. Patek. "Measurement and Correlation of the Surface Tension-Temperature Relation for Methanol." *Journal of Chemical Engineering Data* 53 (2008): 2233-236.

Vignes-Adler, Michele. "Physico-Chemical Aspects of Forced Wetting." *Drop-Surface Interactions*. Ed. Martin Rein. Wien: Springer, 2002.

Zabetakis, M., and D. Burgess. *Research on the Hazards Associated with the Production and Handling of Liquid Hydrogen*. Rep. Pittsburgh: Bureau of Mines, 1961.